On the construction of the Kolmogorov normal form for the Trojan asteroids

Frederic Gabern,[*] **Àngel Jorba**

Departament de Matemàtica Aplicada i Anàlisi, Universitat de Barcelona,

Gran Via 585, 08007 Barcelona, Spain.

Ugo Locatelli

Dipartimento di Matematica, Università degli Study di Roma "Tor Vergata",

Via della Ricerca Scientifica 1, 00133–Roma (Italy).

e-mails: `gabern@mat.ub.es, angel@maia.ub.es, locatell@mat.uniroma2.it`

Abstract

In this paper we focus on the stability of the Trojan asteroids for the planar Restricted Three-Body Problem (RTBP), by extending the usual techniques for the neighbourhood of an elliptic point to derive results in a larger vicinity. Our approach is based on the numerical determination of the frequencies of the asteroid and the effective computation of the Kolmogorov normal form for the corresponding torus. This procedure has been applied to the first 34 Trojan asteroids of the IAU Asteroid Catalog, and it has worked successfully for 23 of them.

The construction of this normal form allows for computer-assisted proofs of stability. To show it, we have implemented a proof of existence of families of invariant tori close to a given asteroid, for a high order expansion of the Hamiltonian. This proof has been successfully applied to three Trojan asteroids.

PACS: 05.10.-a, 05.45.-a, 45.10.-b, 45.20.Jj, 45.50.Pk, 95.10.Ce.

Contents

---

[*]Present Address: Control and Dynamical Systems, California Institute of Technology, Mail Stop 107-81, 1200 East California Blvd, Pasadena, CA 91125, USA.

1　Introduction

The Restricted Three Body Problem (RTBP) models the motion of a particle under the gravitational attraction of two point masses (in our case, Jupiter and Sun) that revolve in circular orbits around their common centre of mass. It is usual to take a rotating reference frame with the origin at the centre of mass, and such that Sun and Jupiter are kept fixed on the x axis, the (x, y) plane is the plane of motion of the primaries, and the z axis is orthogonal to the (x, y) plane. These coordinates are usually called synodical. The (adimensional) units are chosen as follows: the unit of distance is the Sun–Jupiter distance, the unit of mass is the total Sun–Jupiter mass, and the unit of time is such that the period of Jupiter around the Sun equals 2π. With this selection of units, it turns out that the gravitational constant is also equal to 1. Defining momenta as $p_x = \dot{x} - y$, $p_y = \dot{y} + x$ and $p_z = \dot{z}$, the equations of motion for the particle can be written as an autonomous Hamiltonian system with three degrees of freedom (see [Sze67]):

$$H_{RTBP} = \frac{1}{2}(p_x^2 + p_y^2 + p_z^2) + yp_x - xp_y - \frac{1-\mu}{r_{PS}} - \frac{\mu}{r_{PJ}}, \qquad (1)$$

where $\mu = 9.538753600 \times 10^{-4}$ is the mass of Jupiter (in adimensional units), $r_{PS}^2 = (x-\mu)^2 + y^2 + z^2$ is the distance from the particle to the Sun, and $r_{PJ}^2 = (x-\mu+1)^2 + y^2 + z^2$ is the distance from the particle to Jupiter. It is also well known that the RTBP has five equilibrium points (see Figure 1): the collinear points L_1, L_2 and L_3 lay on the x axis and the triangular points L_4 and L_5 form an equilateral triangle (in the (x, y) plane) with Sun and Jupiter. The collinear points are of the type centre×centre×saddle and the triangular points are linearly stable for $\mu < \mu_R = \frac{1}{2}(1 - \sqrt{23/27}) \approx 0.03852$. The nonlinear stability of the triangular points is a much more difficult problem.

Under very general conditions, the well known KAM theorem [Kol54, Arn63, Mos62] (for a survey, see [AKN88] or [Sev03]) can be applied to a small neighbourhood of the Lagrangian points [Leo62, DDB67, Mar71, Mar73, MS86] to ensure the existence of many quasi-periodic motions. Each quasi-periodic trajectory fills densely a compact manifold
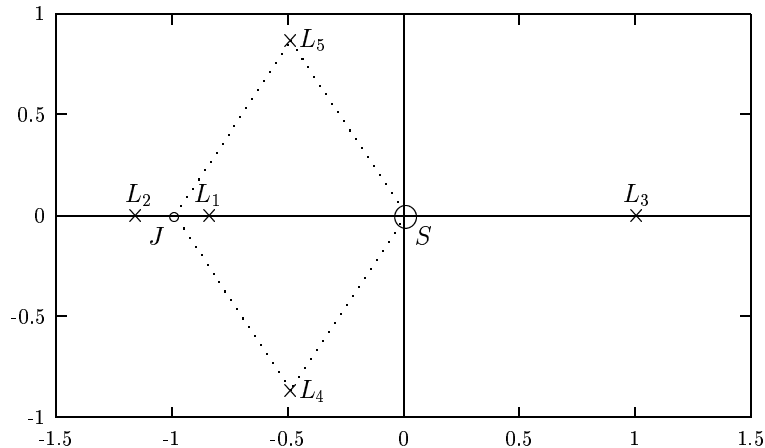
Figure 1: The five equilibrium points of the RTBP.

diffeomorphic to a torus. The union of these invariant tori is a set with positive Lebesgue measure, and empty interior. If the motion of the particle is restricted to the $z = p_z = 0$ plane, then the system only has two degrees of freedom and each torus is a two-dimensional manifold that separates the 3-D energy surface, so it acts as a confiner for the motion –this is the key point in the stability proof for two degrees of freedom Hamiltonian systems–. In the spatial case, the energy manifold is 5-D and the invariant tori are 3-D so that they cannot act as a barrier for the motion. Hence, it may be possible to have trajectories that wander between these tori and escape from any vicinity of an elliptic point. The existence of such trajectories is believed to happen generically in non-integrable Hamiltonian systems. This phenomenon is known as Arnol'd diffusion since it was first conjectured by V.I. Arnol'd in [Arn64].

A different approach to the stability of Hamiltonian systems was introduced by N.N. Nekhoroshev in [Nek77]. The main idea is to derive an upper bound on the diffusion speed on an open domain of the phase space, and to show that the (possible) instability is so slow, that it does not show up in practical applications. These techniques have been applied to derive bounds for the diffusion near the Lagrangian points (see, for instance, [GDF+89, Sim89, CG91, GS97, SD00, GJ01]).

A natural question is the persistence of these stability regions near the Lagrangian points of the Sun-Jupiter system in the real Solar system. In 1906, Max Wolf discovered an asteroid (named 588 Achilles) moving near the L_4 point. Since then, many other asteroids have been found near the triangular points of the Sun-Jupiter system; they are usually called "Trojans", and their names are chosen from Homer's Iliad.

There have been many attempts to rigorously prove the stability of the motion of some of these asteroids in the RTBP with rather limited success. The main difficulty is that these proofs are based on the construction of normal forms at the triangular points, and this is only valid on a small neighbourhood of the point. A different approach is developed in [dlLGJV03]: given an approximation to a quasi-periodic motion (i.e., a nearly invariant torus) it can be shown, under general conditions, the existence of a true invariant torus nearby. Here, the role of the perturbing parameter is played by the accuracy of the

approximated torus: if the error in the invariance condition is small enough, there is a true invariant torus nearby. Moreover, the result does not require the use of action-angle coordinates and, therefore, the hypotheses can be checked, for instance, by means of numerical computations in Cartesian coordinates. The proofs are based on a new iterative scheme that is very suitable for numerics and computer-assisted proofs.

In the present work, we extend the classical techniques for the neighbourhood of an elliptic equilibrium point to derive results in a larger vicinity. As a model, we have used the planar RTBP (by planar we mean the restriction of the RTBP to the invariant manifold $z = p_z = 0$). The initial conditions for the Trojan asteroids are obtained by spherical projection on $z = 0$ from their initial data in the spatial RTBP. Our approach is based on the following scheme:

(a) expand, up to a high order, the Hamiltonian around the triangular points;

(b) perform a low order Birkhoff normal form;

(c) locate a torus in the normal form with the same frequencies as a given Trojan (the frequencies of the Trojan have been previously obtained by a frequency analysis);

(d) translate the origin to this torus;

(e) complete a Kolmogorov normal form up to high order.

Some of the asteroids are rather far from the triangular points and it is not possible to obtain a good approximation for their motion by means of the normal form computed in step (b). In these cases, the algorithm constructing the Kolmogorov normal form is typically divergent, because of numerical instabilities in the determination of the translations, that are requested at step (e). This is a peculiar phenomenon of the RTBP, as we shall discuss later on. To deal with this problem, we will modify steps (d) and (e) to first construct an intermediate object (i.e. a "quasi-invariant" torus) for which a low order Kolmogorov's normalization can be completed, by avoiding the numerical instabilities. Then, if this intermediate object is carefully chosen so that it is close enough to the targeted torus, we can restart from there the complete construction of the Kolmogorov normal form related to the wanted torus (this procedure resembles a numerical "continuation" of the normal form from the equilibrium point to the final torus). We stress that this technique only works for tori that are not too far from the equilibrium point.

With the frequency analysis method ([GMS02, Las99]), we have computed the basic frequencies of the first 34 asteroids of the IAU Asteroid Catalog. Four of these asteroids have a chaotic motion, so we have discarded them. For the remaining 30 asteroids, we have applied the scheme above and succeeded in 23 cases. The 7 failures of the method seem to correspond to asteroids that are too far from the triangular points.

Then, the techniques developed in [LG00] have been adapted to compute the Kolmogorov normal form and to derive a computer assisted proof for the existence of a family of tori very close to a selected asteroid. We remark that the computer assisted proof has been done for a high order expansion of the RTBP, not for the RTBP itself. The main reason is that taking a high order expansion as the initial Hamiltonian makes the computer assisted proof much simpler. On the other hand, the differences between

a high order expansion and the true RTBP are very small (they are quantified later on), much smaller than the differences between the planar RTBP and the real system.

The paper is organized as follows: In Section 2, we describe the preliminary transformations that we make to the RTBP Hamiltonian and how the initial conditions of the Trojan asteroids are obtained from their actual positions and velocities. In Section 3, we use the frequency analysis to make a numerical study of the stability region around the triangular points. In Section 4, the method for constructing invariant tori by means of the Kolmogorov normalization is described. In Section 5, the results of applying this method to the Trojan problem are explained in detail. In Section 6, we discuss the computer-assisted proof of the stability of some of these asteroids based on the KAM theorem. Finally, in Section 7 the conclusions are presented.

2   Description of the model

2.1   Preliminary transformations on the Hamiltonian

It is convenient (see [GS97]) to start by performing a preliminary change to Heliocentric polar coordinates. We translate the origin from the center of masses to the Sun, and we introduce polar coordinates by means of the following change of variables:

$$
\begin{array}{llll}
x & = & \rho\cos\theta + \mu, & p_x & = & p_\rho\cos\theta - \frac{\sin\theta}{\rho}p_\theta, \\
y & = & \rho\sin\theta, & p_y & = & p_\rho\sin\theta + \frac{\cos\theta}{\rho}p_\theta + \mu.
\end{array}
\tag{2}
$$

Afterwards, we take local coordinates (X, Y, P_X, P_Y) centered in the L_4 or L_5 triangular points by performing the following translation:

$$
\begin{array}{llll}
\rho & = & X + 1, & p_\rho & = & P_X, \\
\theta & = & Y + \pi \pm \frac{\pi}{3}, & p_\theta & = & P_Y + 1,
\end{array}
$$

where the positive sign in the second equation corresponds to L_4 and the negative sign to L_5. In this new variables, the Hamiltonian takes the form:

$$
\begin{aligned}
H(X, Y, P_X, P_Y) & = & \frac{1}{2}\left[P_X^2 + \frac{(P_Y + 1)^2}{(X + 1)^2}\right] - P_Y \\
& & -\mu(X + 1)\cos(Y + \pi \pm \frac{\pi}{3}) - \frac{1 - \mu}{X + 1} \\
& & -\frac{\mu}{\sqrt{(X + 1)^2 + 1 + 2(X + 1)\cos(Y + \pi \pm \frac{\pi}{3})}}.
\end{aligned}
\tag{3}
$$

Note that from a solution $(X(t), Y(t), P_X(t), P_Y(t))$ close to L_4 we can derive another one, $(\tilde{X}(t), \tilde{Y}(t), \tilde{P}_X(t), \tilde{P}_Y(t))$, close to L_5 (and vice versa) through the symmetry $(\tilde{X} = X, \tilde{Y} = -Y, \tilde{P}_X = P_X, \tilde{P}_Y = -P_Y)$. Therefore, it is enough to study a neighbourhood of the L_5 point so that we will use the Hamiltonian (3) with the minus sign and, if the considered asteroid is close to L_4, we will apply this symmetry to work in a neighbourhood of L_5.

2.2 Normalization of the quadratic part of the Hamiltonian

Skipping a constant term, the previous Hamiltonian can be expanded around L_5 as a real power series of the form,

$$H(X, Y, P_X, P_Y) = \sum_{l=2}^{+\infty} f_l(X, Y, P_X, P_Y),$$

where $\forall l \geq 2$, $f_l(X, Y, P_X, P_Y) \in \mathcal{P}_l(X, Y, P_X, P_Y)$ and $\mathcal{P}_l(\cdot)$ is the space of homogeneous polynomials of degree l in the variables appearing as arguments. It is well known that, if $\mu < (1 - \sqrt{23/27})/2$, there is a class of linear canonical transformations $(X, Y, P_X, P_Y) = \mathcal{L}(x_1, x_2, y_1, y_2)$ bringing the quadratic part of the Hamiltonian in normal form,

$$H^{(\mathrm{I})}(x_1, x_2, y_1, y_2) = \frac{\nu_1}{2}(x_1^2 + y_1^2) + \frac{\nu_2}{2}(x_2^2 + y_2^2) + \sum_{l=3}^{+\infty} f_l^{(\mathrm{I})}(x_1, x_2, y_1, y_2), \qquad (4)$$

where $f_l^{(\mathrm{I})}(x_1, x_2, y_1, y_2) \in \mathcal{P}_l(x_1, x_2, y_1, y_2)$, $\forall l \geq 3$. One of these canonical transformations can be calculated as described in Section 2.1 of [GS97] (where the linear transformation used in [GDF$^+$89] is adapted to the polar coordinates introduced in (2)). We remark that here we have used a canonical transformation $\mathcal{L}$ that is not the same as the one described in [GS97] and that the results in the present work do not depend on this choice. In the Sun-Jupiter system , we have $\mu = 9.538753571 \times 10^{-4}$ and the frequencies take the values:

$$\nu_1 = -8.0463875714716596 \times 10^{-2}, \qquad \nu_2 = 9.9675752553214603 \times 10^{-1}. \qquad (5)$$

We introduce action-angle variables by means of the canonical transformation $(x, y) = \mathcal{A}(I, \varphi)$ defined as:

$$x_j = \sqrt{2I_j} \cos \varphi_j, \quad y_j = \sqrt{2I_j} \sin \varphi_j, \quad \forall\, j = 1, \ldots, n, \qquad (6)$$

where hereafter we write the expressions of the canonical transformations for a system having generically n degrees of freedom (of course, in the planar RTBP, $n = 2$). Then, the Hamiltonian can be written as

$$H^{(\mathrm{II})}(I, \varphi) = \nu \cdot I + \sum_{l=3}^{+\infty} f_l^{(\mathrm{II})}(I, \varphi), \qquad (7)$$

where the functions $f_l^{(\mathrm{II})}$ are homogeneous polynomials of degree l in the square root of the actions and trigonometric polynomials of degree l in the angles. Moreover, for any fixed index $m \in \{1, \ldots, n\}$ and for all term appearing in the expansion of $f_l^{(\mathrm{II})}$ the degree
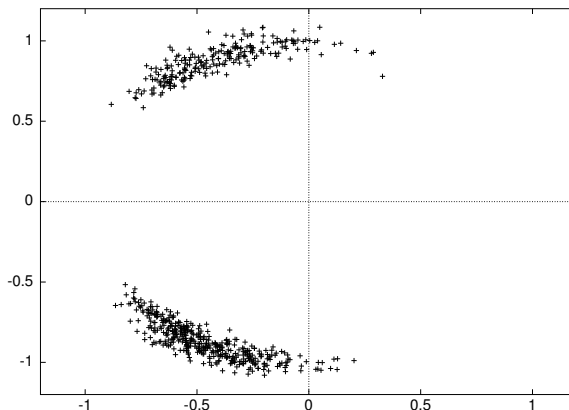
Figure 2: Spherical projection into the (x, y) coordinates of the planar RTBP Sun-Jupiter system of the Trojan orbital elements at the Julian date 2452600.5. Note how these initial conditions shadow the banana shape of the stability region.

in $\sqrt{I_m}$ and the m-th component of the Fourier harmonics have the same parity, i.e.

$$
\begin{aligned}
f_l^{(\mathrm{II})}(I, \varphi) \;=\; & \sum_{i_1+\ldots+i_n=l} \sum_{j_1=0}^{i_1} \cdots \sum_{j_n=0}^{i_n} \Bigg\{ \\
& c_{i_1,\ldots,i_n,j_1,\ldots,j_n}^{(\mathrm{II})} \left(\prod_{m=1}^{n} \sqrt{I_m^{i_m}} \right) \cos \left[\sum_{m=1}^{n} (i_m - 2j_m)\varphi_m \right] \\
& + d_{i_1,\ldots,i_n,j_1,\ldots,j_n}^{(\mathrm{II})} \left(\prod_{m=1}^{n} \sqrt{I_m^{i_m}} \right) \sin \left[\sum_{m=1}^{n} (i_m - 2j_m)\varphi_m \right] \Bigg\},
\end{aligned} \tag{8}
$$

where $c_{i_1,\ldots,i_n,j_1,\ldots,j_n}^{(\mathrm{II})}$ and $d_{i_1,\ldots,i_n,j_1,\ldots,j_n}^{(\mathrm{II})}$ are real coefficients.

The action-angle coordinates (I, φ) and the Hamiltonian (7) are the usual setting to use the tools of the perturbation theory (Birkhoff normal form, KAM and Nekhoroshev theory, etc.).

2.3 Initial conditions of the Trojan asteroids in the planar RTBP

The orbital elements of the Trojan asteroids are taken from the Bowell Catalog [Bow] at the Julian date 2452600.5 (October 22th, 2002). Afterwards, we send their coordinates to the three dimensional RTBP system and, finally, we project them spherically to the Sun-Jupiter plane to obtain the initial conditions to be used in the computations. We believe that to simulate the Trojan asteroids in the planar RTBP, a spherical projection (which is equivalent to take zero inclinations) makes more sense than an orthogonal projection w.r.t. the z axis. In Figure 2, we plot the synodical (x, y) coordinates corresponding to these initial conditions for the RTBP system. It is remarkable how these projected coordinates shadow the famous "banana" shape of the stability region found in several numerical investigations ([MS81]).
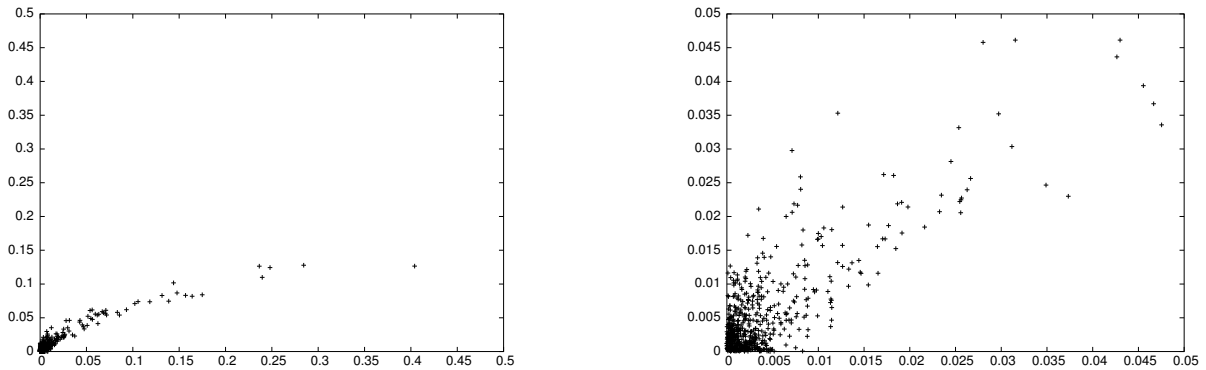
Figure 3: (I_1, I_2) spherical projections of the Trojan initial conditions into the Sun-Jupiter plane in the Julian date 2452600.5. The right plot is a zoom of the left plot's left-bottom corner.
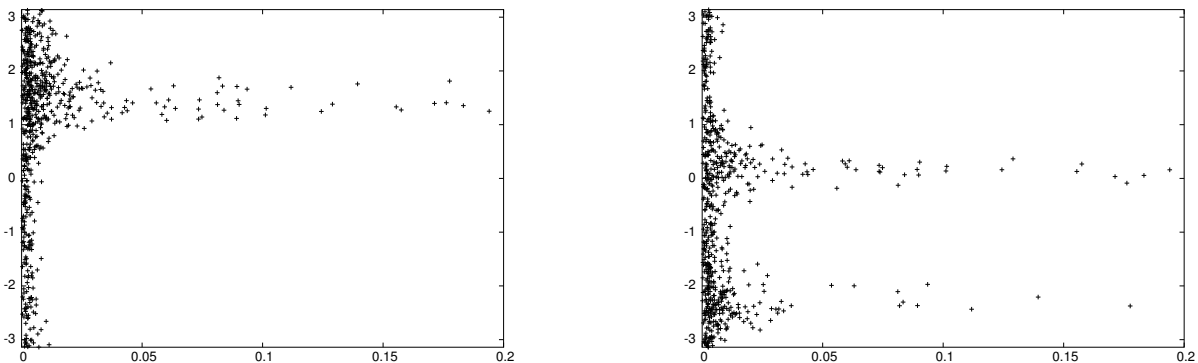

Figure 4: Measure of the distance to the Lagrangian point ($\|I\|_2 = \sqrt{I_1^2 + I_2^2}$) of the Trojans' projected coordinates. The left plot corresponds to $(\|I\|_2, \varphi_1)$ and the right one to $(\|I\|_2, \varphi_2)$.

In Figure 3, the distribution of these initial conditions in the (I_1, I_2) plane is shown. We can see that most of them lie in the domain $\max\{I_1, I_2\} \leq 0.05$, but it is worth to note that some of them reach very high action values ($I_1 \gg 0.1$). This fact makes very difficult to use perturbative methods around the equilibrium point, $I_1 = I_2 = 0$, to prove stability for such distant objects.

In Figure 4, we plot a measure of the distance (given by $\|I\|_2 = \sqrt{I_1^2 + I_2^2}$) of these initial conditions to the triangular points with respect to the two angles (φ_1, φ_2), where the action-angle variables are defined by (6). This figure suggests that for some particular phases (e.g. $\varphi_1 \sim 1.3$ or 1.7 and $\varphi_2 \sim 0.3$ or -2.5), the stability regions are larger. The asteroids that reach higher values of the actions can go farther from the equilibrium points. In particular, they correspond to the bodies that can approach the extremes of the banana region mentioned before. In the next section we confirm these assertions with a numerical simulation of the "global" dynamics near the triangular region for some concrete phases.

3 Numerical study of the stability region

We fix the variables φ_1 and φ_2 (the concrete values will be specified later on) and we take a mesh of points in the positive quadrant of the (I_1, I_2) plane:

$$
\begin{aligned}
I_1 &= \frac{k_1 I_1^{max}}{N_1} \quad \text{for } k_1 = 0, \ldots, N_1, \\
I_2 &= \frac{k_2 I_2^{max}}{N_2} \quad \text{for } k_2 = 0, \ldots, N_2.
\end{aligned}
$$

We use these points, $(I_1, I_2, \varphi_1, \varphi_2)$, as initial conditions of a numerical integration in a interval of time $[0, T]$. The integration is performed by the symplectic integrator $\mathcal{SBAB}_3$ (described in [LR01]) with a fixed time step of 0.005 and with $T = 2^{15} = 32768$ (in adimensional units). Then, by means of a refined Fourier analysis of a sample of the trajectory (see [GMS02], for the actual implemented algorithm, and [Las95, Las99], for an introduction to the frequency analysis method), we evaluate the two basic frequencies of the orbits that we call $\omega_1^{(1)}$ and $\omega_2^{(1)}$. Afterwards, we repeat the integration in the interval of time $[T, 2T]$ and we recompute the frequencies. In this case, we call them $\omega_1^{(2)}$ and $\omega_2^{(2)}$. Finally, we consider the values $\delta_j = \left|1 - \omega_j^{(2)}/\omega_j^{(1)}\right|$, $j = 1, 2$, as an estimation of the diffusion rate (see [RL01]) related to the orbit starting from the phase space point $(I_1, I_2, \varphi_1, \varphi_2)$. The value of δ_j gives an estimation of the chaoticity of the particular orbit. That is, if the trajectory associated to an initial condition is quasi-periodic, δ_j should be zero.

In Figure 5, we show a contour plot of the function $\sigma_j = \log \delta_j$ for $j = 1$ (we obtain similar pictures for the σ_2 case). The color code goes from blue, corresponding to motion close to quasi-periodic ($\delta_j < 10^{-10}$), to red, for strongly irregular and escaping motion ($\delta_j > 10^{-2}$). We plot two examples corresponding to the selection of two pairs of phases: $(\varphi_1, \varphi_2) = (0, 0)$ (left plot) and $(\varphi_1, \varphi_2) = (1.78, -2.82)$ (right plot). The stability region (blue part) shown in the left plot is the generic situation for most of the phases. But, for some particular initial phases the stability region is much larger. This is the case in the right plot, where we choose a phase very close to the one of the asteroid 2759-Idomeneus (which has a rather large $\|I\|_2$).

Let us compare the existing analytical results with the stability region given by our numerical investigations. Looking at Table 1 of both [GS97] and [SD00] (that contain, up to our knowledge, the best existing results of the Trojan stability in the RTBP model) the domain of the initial conditions corresponding to orbits that are effectively stable is approximately contained in the rectangle $(I_1, I_2) \in [0, 0.0005] \times [0, 0.0008]$. This fact clearly shows that the analytical results obtained up to now are quite far from giving a complete explanation of the stability of the motion of the Trojans.
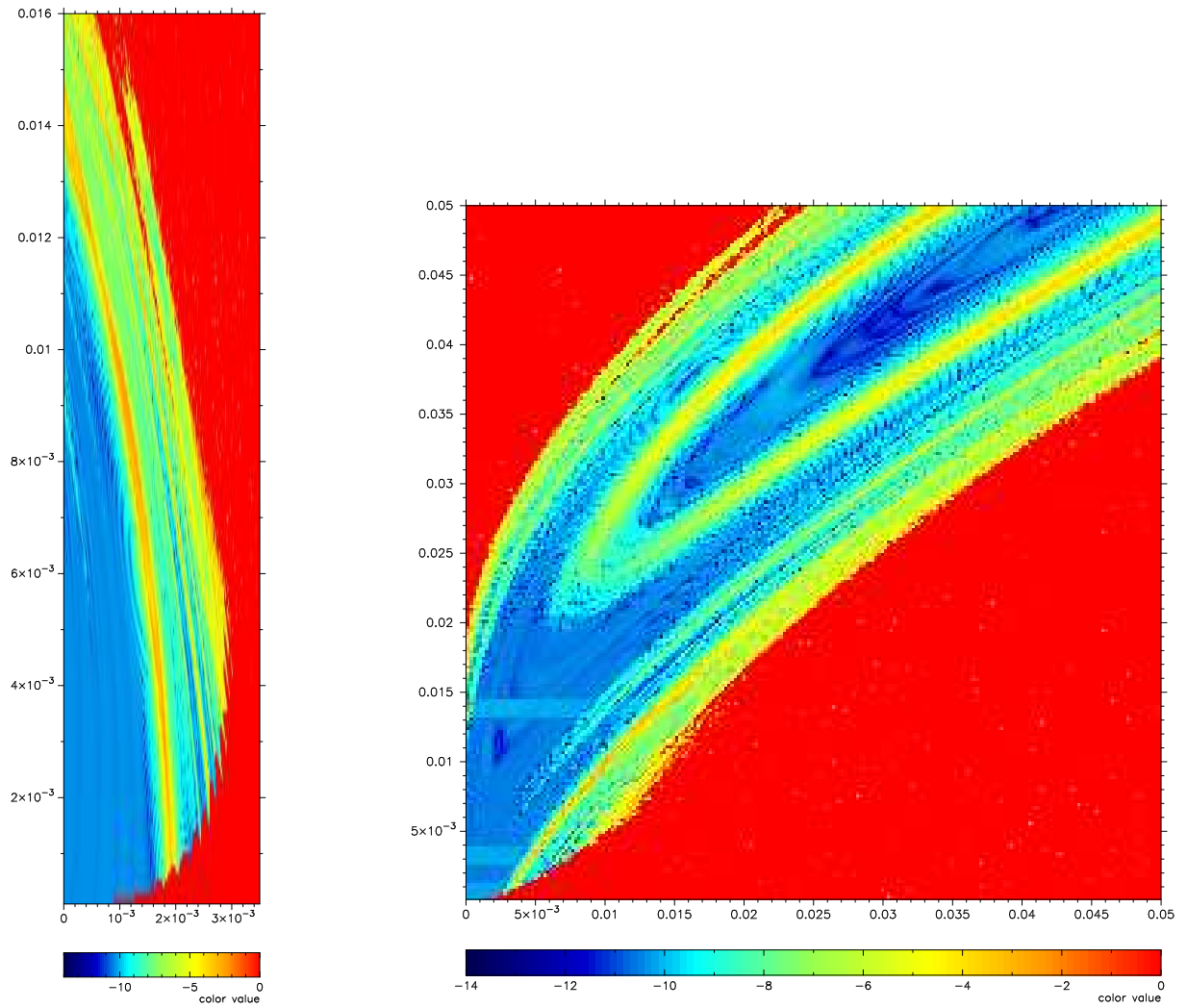
Figure 5: Global stability portrait of the (I_1, I_2) plane for two different pairs of phases. The left plot corresponds to the phases $(\varphi_1, \varphi_2) = (0, 0)$. The phases for the right plot are $(\varphi_1, \varphi_2) = (1.78, -2.82)$. See text for more details.

4 Constructive algorithm for invariant tori close to an elliptic point

An explicit procedure to construct invariant tori near an elliptic equilibrium point is described in [LG00], where the considered system is the secular part of the Sun–Jupiter–Saturn system. The algorithm can also be applied to the neighbourhood of the Lagrangian points of the RTBP, but it only converges for initial data in a domain that has more or less the same size as the set of initial condition for which the method used in [GS97] and in [SD00] works. In the present section, we will explain how such a procedure can be modified in order to increase its domain of application. Therefore, in Section 4.1 we first adapt the algorithm described in [LG00] to the present context. In Section 4.2 we provide an example that illustrates why a direct application of that algorithm to the RTBP gives poor results. Finally, in Section 4.3 we show the modifications that will allow us to construct invariant tori in a much wider neighbourhood of the equilibrium point.

4.1 Kolmogorov's normalization near an elliptic equilibrium point

The goal is to introduce a suitable set of coordinates such that (7) is in the Kolmogorov's normal form,

$$H^{(\infty)}(p, q) = \omega \cdot p + \mathcal{O}(p^2) \ , \tag{9}$$

where the surface $p = 0$ is invariant with respect to the flow and the motion over that torus has angular frequencies equal to $\omega \in \mathbb{R}^n$. The algorithm consists of a sequence of canonical transformations that we describe in three separated steps.

(i) *Birkhoff normalization up to a finite degree*
The aim of each single step of the Birkhoff normalization is to eliminate the dependence on the angles in the part of the Hamiltonian having a fixed degree in the (square root of the) actions. To be more precise, let us describe the Birkhoff normalization of the third degree. We first determine a generating function $B^{(\mathrm{III})}$ by solving the equation

$$\nu \cdot \frac{\partial B^{(\mathrm{III})}}{\partial \varphi} + f_3^{(\mathrm{II})} - \langle f_3^{(\mathrm{II})} \rangle_\varphi = 0 \ , \tag{10}$$

where $\langle \cdot \rangle_\varphi$ indicates the average over the angles φ. From the generic form of the functions $f_l^{(\mathrm{II})}$ described in (8), it follows that $\langle f_3^{(\mathrm{II})} \rangle_\varphi = 0$. Using the formalism of the Lie series (for an introduction to these topics, see, e.g., [Grö60] and [Gio95]), the transformed Hamiltonian is given by

$$H^{(\mathrm{III})} = \exp L_{B^{(\mathrm{III})}} H^{(\mathrm{II})} = \sum_{j=0}^{+\infty} \frac{1}{j!} L_{B^{(\mathrm{III})}}^j H^{(\mathrm{II})} = \nu \cdot I + \sum_{l=4}^{+\infty} f_l^{(\mathrm{III})}(I, \varphi) \ , \tag{11}$$

where we have renamed the new variables of $H^{(\mathrm{III})}$ again (I, φ) (this abuse of notation will be repeated hereafter) and one can easily calculate the expression of $f_l^{(\mathrm{III})}$ as a function of $B^{(\mathrm{III})}$ and $f_l^{(\mathrm{II})}$ just collecting the homogeneous polynomials having the same degree in the square root of the actions. Thus, the functions $f_l^{(\mathrm{III})}$ are of the same type as in (8).

It is well known that this sequence of Hamiltonians and canonical transformations produced by the Birkhoff normalization does not converge on any open neighbourhood of the equilibrium point ([PM03]). Note that the Birkhoff normal form of degree 3 is enough to start the following construction of the Kolmogorov's normal form and that the radius of convergence of the Hamiltonian shrinks to zero when the degree of the Birkhoff normalization goes to ∞. On the other hand, by performing the Birkhoff normalization up to a degree higher than 3, we can improve the numerical stability of the calculation of the coefficients appearing in the expansions generated by the algorithm. Here, we have computed the Birkhoff normalization up to fifth degree which is good enough for our purposes.

To fix the ideas, let us conclude describing the construction of the Birkhoff normal form up to the fifth degree. The final Hamiltonian is given by

$$
\begin{aligned}
H^{(\mathrm{V})} &= \exp L_{B^{(\mathrm{V})}} \Big(\exp L_{B^{(\mathrm{IV})}} \big(\exp L_{B^{(\mathrm{III})}} H^{(\mathrm{II})} \big) \Big) \\
&= \nu \cdot I + f_4^{(\mathrm{V})}(I) + \sum_{l=6}^{+\infty} f_l^{(\mathrm{V})}(I, \varphi) \ ,
\end{aligned} \tag{12}
$$

where (a) the functions $f_l^{(\mathrm{V})}$ are homogeneous polynomials of degree l in the square root of the actions I of type (8); (b) the generating function $B^{(\mathrm{IV})}$ is defined by the following equation:

$$
\nu \cdot \frac{\partial B^{(\mathrm{IV})}}{\partial \varphi} + f_4^{(\mathrm{III})} - \langle f_4^{(\mathrm{III})} \rangle_\varphi = 0 \ ; \tag{13}
$$

(c) the generating function $B^{(\mathrm{V})}$ is obtained by solving an analogous equation where terms of fifth degree in the square root of the actions and with angular average equal to 0 appear; and finally, (d) $f_4^{(\mathrm{V})} = \langle f_4^{(\mathrm{III})} \rangle_\varphi$.

Let us recall that the canonical transformation $\mathcal{B}$ inducing the Birkhoff normalization up to the fifth degree is explicitly given by

$$
\mathcal{B}(I, \varphi) = \exp L_{B^{(\mathrm{V})}} \Big(\exp L_{B^{(\mathrm{IV})}} \big(\exp L_{B^{(\mathrm{III})}} (I, \varphi) \big) \Big) \ , \tag{14}
$$

because one immediately sees that $H^{(\mathrm{V})}(I, \varphi) = H^{(\mathrm{II})}\big(\mathcal{B}(I, \varphi)\big)$ using the exchange theorem for Lie series.

(ii) *Initial translation of the actions*
The canonical transformation $(I, \varphi) = \mathcal{T}(p, q)$ performing a translation of the actions is of the following type:

$$
I_j = p_j + I_j^* \ , \qquad \varphi_j = q_j \ , \qquad \forall \, j = 1, \ldots, n \ . \tag{15}
$$

Let us recall that we are constructing an invariant torus with a fixed frequency vector ω. Following [LG00], the initial translation can be determined in such a way that, *in the integrable approximation*, the quasi-periodic motions on the invariant torus $(p = 0, q \in \mathbb{T}^n)$ have angular frequencies ω. Therefore, we determine the vector I^* with positive components (recall the canonical transformation in (6)) as the nearest to the origin solution of

the following equations:

$$\nu_j + \frac{\partial f_4^{(\mathrm{V})}}{\partial I_j}(I) + \frac{\partial \langle f_6^{(\mathrm{V})} \rangle_\varphi}{\partial I_j}(I) = \omega_j \ , \qquad \forall \, j = 1, \ldots, n \ . \tag{16}$$

We can write the expansion of $H^{(\mathrm{VI})}(p,q) = H^{(\mathrm{V})}(\mathcal{T}(p,q))$ as follows:

$$H^{(\mathrm{VI})}(p,q) = \omega \cdot p + \sum_{s \geq 0} \sum_{l \geq 0} f_l^{(\mathrm{VI},s)}(p,q) \ , \tag{17}$$

where $f_l^{(\mathrm{VI},s)} \in \mathcal{P}_{l,2s}$ and $\mathcal{P}_{l,2s}$ is the set of functions that are homogeneous polynomials of degree l in the action variables and trigonometric polynomials of degree $2s$ in the angular ones. Note that this expansion is unique if we add the request that any monomial term appearing in the explicit expression of $f_l^{(\mathrm{VI},s+1)}$ cannot belong to $\mathcal{P}_{l,2s}$, $\forall \, l \geq 0$ and $s \geq 0$. Moreover, using the Cauchy inequalities, one easily sees that the size (of any suitable norm) of $f_l^{(\mathrm{VI},s)}$ can be estimated with an upper bound that is essentially proportional to the s–th power of the ratio of $\|I^*\|$ over the analytic radius of convergence of $H^{(\mathrm{V})}$, and it is inversely proportional to the l–th power of the minimum component of vector I^* (see the discussion in [Loc01]).

At this point, we want to mention that we have some freedom in the crucial choice of the initial translation vector I^*, as it will be discussed in Section 4.3.

(iii)*The standard Kolmogorov's normalization algorithm*
Let us describe the generic r–th step of the Kolmogorov's normalization algorithm. We begin with a Hamiltonian of the type

$$H^{(r-1)}(p,q) = \omega \cdot p + \sum_{s \geq 0} \sum_{l \geq 0} f_l^{(r-1,s)}(p,q) \ , \tag{18}$$

where $f_l^{(r-1,s)} \in \mathcal{P}_{l,2s}$ and none of the monomials in the expansion of $f_l^{(r-1,s+1)}$ belong to $\mathcal{P}_{l,2s}$, $\forall \, l \geq 0$ and $s \geq 0$. To fix the ideas, we can start with $r = 2$ defining $H^{(1)} = H^{(\mathrm{VI})}$.

Since we point to a Hamiltonian of type (9), we must remove the main perturbing terms of degree 0 and 1 in the actions. We will proceed in two separate steps. We first remove part of the unwanted terms via a canonical transformation with generating function $\chi_1^{(r)}(q) = X^{(r)}(q) + \xi^{(r)} \cdot q$ (being $\xi^{(r)} \in \mathbb{R}^n$). Thus, we solve with respect to $X^{(r)}(q)$ and $\xi^{(r)}$ the equations

$$\omega \cdot \frac{\partial X^{(r)}}{\partial q}(q) + \sum_{s=1}^{r} f_0^{(r-1,s)}(q) = 0 \ , \quad C^{(r)} \xi^{(r)} \cdot p + f_1^{(r-1,0)}(p) = 0 \ , \tag{19}$$

where the $n \times n$ matrix $C^{(r)}$ is defined by the equation $\frac{1}{2} C^{(r)} p \cdot p = f_2^{(r-1,0)}(p)$. A unique solution satisfying $\langle X^{(r)} \rangle_q = 0$ exists if the frequencies ω are non–resonant up to order $2r$, $k \cdot \omega \neq 0$, $\forall \, 0 < |k| \leq 2r$ with $k \in \mathbb{Z}^n$, and if $\det C^{(r)} \neq 0$. We must now give the expressions of the functions $\hat{f}_l^{(r,s)}$ appearing in the expansion of the new Hamiltonian:

$$\hat{H}^{(r)}(p,q) = \omega \cdot p + \sum_{s \geq 0} \sum_{l \geq 0} \hat{f}_l^{(r,s)}(p,q) \ , \tag{20}$$

where $\hat{H}^{(r)} = \exp L_{\chi_1^{(r)}} H^{(r-1)}$. To this aim, we will redefine many times the same quantity without changing the symbol. In our opinion, such a repeated abuse of notation has two advantages: first, this makes easier to understand the final calculation of $\hat{f}_l^{(r,s)}$ instead of using one single very complicated formula; second, the description of the algorithm is more similar to its translation in a programming code. For instance, mimicking the C language, with the notation $a \hookleftarrow b$ we mean that the previously defined quantity a is redefined as $a = a + b$. Therefore, we initially define

$$\hat{f}_l^{(r,s)} = f_l^{(r-1,s)}(p,q) \quad \forall \, l \geq 0 \text{ and } s \geq 0 . \tag{21}$$

To take into account the Poisson bracket of the generating function with $\omega \cdot p$, we put

$$\hat{f}_0^{(r,0)} \hookleftarrow \omega \cdot \xi^{(r)} , \qquad \hat{f}_0^{(r,s)} = 0 \quad \forall \, 1 \leq s \leq r . \tag{22}$$

Then, we consider the contribution of the terms generated by the Lie series applied to each function $f_l^{(r-1,s)}$ as follows:

$$\hat{f}_{l-j}^{(r,s+jr)} \hookleftarrow \frac{1}{j!} L_{\chi_1^{(r)}}^j f_l^{(r-1,s)} \quad \forall \, l \geq 1 , \ s \geq 0 \text{ and } 1 \leq j \leq l . \tag{23}$$

Looking at formulæ (21)–(23), one can easily check that $\hat{f}_l^{(r,s)} \in \mathcal{P}_{l,2s} \ \forall \, l \geq 0$ and $s \geq 0$. We perform now a *"reordering of the terms"*: this means that for any fixed $\hat{f}_l^{(r,s)}$ we move to $\hat{f}_l^{(r,j)}$ all the monomials appearing in its expansion and belonging also to $\mathcal{P}_{l,2j}$ with $0 \leq j < s$; we repeat this operation on Hamiltonian (20) in such a way that at the end of the reordering none of the monomials in the expansion of $\hat{f}_l^{(r,s+1)}$ belong to $\mathcal{P}_{l,2s}$, $\forall \, l \geq 0$ and $s \geq 0$.

In the second part of the r–th step of the Kolmogorov's normalization algorithm, by using another canonical transformation, we remove the part of the perturbation up to the order of magnitude r that actually depends on the angles and it is linear in the actions. Thus, we solve with respect to $\chi_2^{(r)}(p,q)$ the equation

$$\omega \cdot \frac{\partial \chi_2^{(r)}}{\partial q}(p,q) + \sum_{s=1}^{r} \hat{f}_1^{(r,s)}(p,q) = 0 , \tag{24}$$

where again the solution exists and it is unique if $\langle \chi_2^{(r)} \rangle_q = 0$ and the frequencies ω are non–resonant up to order $2r$. Analogously to what we have done above, we now provide the expressions of the functions $f_l^{(r,s)}$ appearing in the expansion of the new Hamiltonian:

$$H^{(r)}(p,q) = \omega \cdot p + \sum_{s \geq 0} \sum_{l \geq 0} f_l^{(r,s)}(p,q) , \tag{25}$$

where $H^{(r)} = \exp L_{\chi_2^{(r)}} \hat{H}^{(r)}$. We initially define

$$f_l^{(r,s)} = \hat{f}_l^{(r,s)}(p,q) \quad \forall \, l \geq 0 \text{ and } s \geq 0 . \tag{26}$$

In order to take into account the contribution of the terms generated by the Lie series applied to $\omega \cdot p$, we put

$$f_1^{(r,jr)} \hookleftarrow \frac{1}{j!} L_{\chi_2^{(r)}}^{j-1} \left(\omega \cdot \frac{\partial \chi_2^{(r)}}{\partial q} \right) \qquad \forall \, j \geq 1 \, . \tag{27}$$

Then, the contribution of the Lie series applied to the rest of the Hamiltonian $\hat{H}^{(r)}$ implies that

$$f_l^{(r,s+jr)} \hookleftarrow \frac{1}{j!} L_{\chi_2^{(r)}}^{j} \hat{f}_l^{(r,s)} \qquad \forall \, l \geq 0 \, , \; s \geq 0 \text{ and } j \geq 1 \, . \tag{28}$$

Finally, we perform a new *"reordering of the terms"*, so that at the end the functions $f_l^{(r,s)} \in \mathcal{P}_{l,2s}$ appearing in the expansion (25) of the new Hamiltonian $H^{(r)}$ are such that none of the monomials in the expansion of $f_l^{(r,s+1)}$ belong to $\mathcal{P}_{l,2s}$, $\forall \, l \geq 0$ and $s \geq 0$. Let us recall that the canonical transformation $\mathcal{K}^{(r)}$ inducing the Kolmogorov's normalization up to the step r is explicitly given by

$$\mathcal{K}^{(r)}(p,q) = \exp L_{\chi_2^{(r)}} \left(\exp L_{\chi_1^{(r)}} \left(\dots \exp L_{\chi_2^{(2)}} \left(\exp L_{\chi_1^{(2)}} (p,q) \right) \dots \right) \right). \tag{29}$$

This conclude the r–th step of the algorithm that can be iterated at the next step.

Let us end the description of the standard Kolmogorov's normalization with a final remark. As a main difference with respect to other papers on the KAM theory (i.e. [GL97a], [GL97b], [CGL00] and [LG00]), here we have not explicitly written the expansions in a small parameter, instead we have clearly prescribed to add up terms corresponding to different orders of magnitude in the small parameter when the *"reordering of the terms"* is performed. The main advantage of this slight modification is to save most of the memory occupation when the calculations are performed on a computer. Roughly speaking, it is possible to handle the temporarily defined functions in such a way that, for any fixed degree l, one can keep in memory the expansion requested by one single function $\in \mathcal{P}_{l,2s}$ instead of that requested by a function $\in \mathcal{P}_{l,2}$, plus one $\in \mathcal{P}_{l,4}$, $\dots$, plus one $\in \mathcal{P}_{l,2s}$. This is an important improvement, because the final accuracy of the results depends on the number of Kolmogorov's normalization steps that one can explicitly perform on the computer (see the discussions about both the study of the approximation of the orbits and the computer–assisted proofs of existence of KAM tori in [LG00] and [CGL00], respectively.).

4.2 Non uniqueness of invariant tori for fixed frequency vectors

As it has been mentioned before, a straightforward application of the Kolmogorov's normalization algorithm gives disappointing results. Indeed, when the initial translation vector I^* is not very small, the sequence of the canonical transformations is non-convergent. In particular, the first generating functions that show up a sudden increase of the coefficients in the numerical implementation of the method, is the translation of the actions, i.e. $\{\xi^{(r)} \cdot q\}_{r \geq 2}$. Here we will discuss some of the reasons for such a behavior.
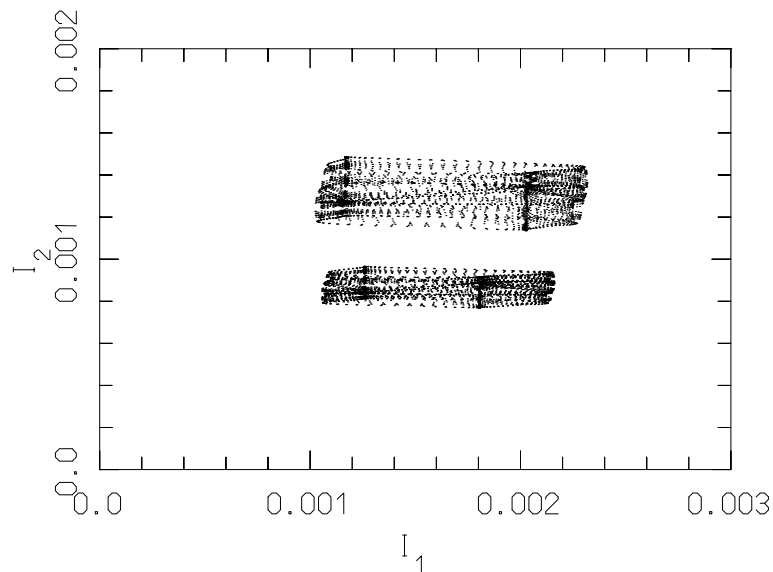
Figure 6: Projection on the plane (I_1, I_2) of the shape of two different invariant tori having the same angular frequencies. The lower torus is given by the algorithm described at points (a)–(e) of 4.3, starting from the frequencies $(\omega_1, \omega_2) = (-0.0787481844821318, 0.996540006111648)$ corresponding to 624 Hektor (see Table 1). The upper torus is obtained by changing the previous algorithm at the point (b_1) only: in this second case, we used the nearest to the origin solution of (16) as the initial translation vector I^*. In both cases, we projected $5\,000$ equally time-spaced points along the motion $(p(t) = 0, q(t) = \omega t)$ (where (p, q) are the action-angle coordinates at the end of the normalization procedure) through the canonical transformations $\mathcal{B} \circ \mathcal{T} \circ \mathbf{K}^{(20)} \circ \mathcal{K}^{(20)}$ related to the two different invariant tori (with $\mathcal{B}$, $\mathcal{T}$, $\mathbf{K}^{(20)}$ and $\mathcal{K}^{(20)}$ defined as in 4.3).

First of all, let us recall that the vectors $\xi^{(r)}$ are determined by the second equation in (19), where the matrix $C^{(r)}$ gives approximately (in the limit $r \to \infty$) the local correspondence between frequencies and actions, in a set of coordinates such that the action values locate the invariant tori (see [MG95]).

Figure 6 shows two different tori with the same frequencies. Moreover, we have checked that the determinants of the two matrices $C^{(\infty)}$ related to those two tori have opposite signs – one can prove that the determinant of the matrix $C^{(\infty)}$ is an intrinsic function of the invariant torus and is invariant under canonical transformations for which the origin is fixed. Therefore, it does not exist a one-to-one mapping between frequencies and invariant tori.

As discussed in [Las99], in the context of quasi-integrable systems, the frequency analysis can be used to describe the diffeomorphism $\Psi : \mathbf{T}^n \times \Omega \mapsto \mathbf{T}^n \times \mathbf{R}^n$ (where Ω is a suitable open set of frequencies) such that its restriction on a Cantor subset $\tilde{\Omega} \subset \Omega$ locate the invariant tori; i.e. the manifold $\Psi(\mathbf{T}^n, \omega)$ is invariant $\forall\, \omega \in \tilde{\Omega}$. The existence and regularity of Ψ were proved in [Pös82].

In Figure 7, we numerically study the correspondence between the actions (I_1, I_2), before the Birkhoff normalization, and the frequencies of the motion (ω_1, ω_2). More concretely, we investigate the Jacobian, J, of $\Phi_\varphi(\cdot) = \Psi^{-1}(\varphi, \cdot)$, where the values of the angles $\varphi = (\varphi_1, \varphi_2)$ are fixed. This figure highlights the existence of a manifold where $\det J = 0$. Therefore, in this case, the correspondence between frequencies and invariant tori is not invertible.

This is related to the numerical instability of the determination of the translations of the actions, $\{\xi^{(r)} \cdot q\}_{r \geq 2}$. Let us note that in the algorithm described in Section 4.1, the determinants of the matrix $C^{(\infty)}$ and the Jacobian J are nearly equal. Indeed, the construction of the Kolmogorov's normal form that starts with coordinates $(I_1, I_2, \varphi_1, \varphi_2)$ is given by the composition of:

1. the Birkhoff normalization $\mathcal{B}$, which is near to the identity in a neighborhood of the origin of the actions;

2. the initial translation of the actions $\mathcal{T}$, that does not change the Jacobian of the frequencies–actions map;

3. the standard Kolmogorov's normalization algorithm, that uses matrices related to $C^{(\infty)}$.

Thus, the determinant of $C^{(r)}$ can get very small (possibly zero) when dealing with the normalization algorithm, even for invariant tori located not far from the equilibrium point. We believe that this fact explains the strong numerical instability observed in the determination of the sequence of vectors $\xi^{(r)}$.

4.3   The modified algorithm constructing the Kolmogorov's normal form

As the prediction of the translation vectors $\xi^{(r)}$ given by (19) can be affected by large errors, we have split the standard Kolmogorov's normalization algorithm in two separate
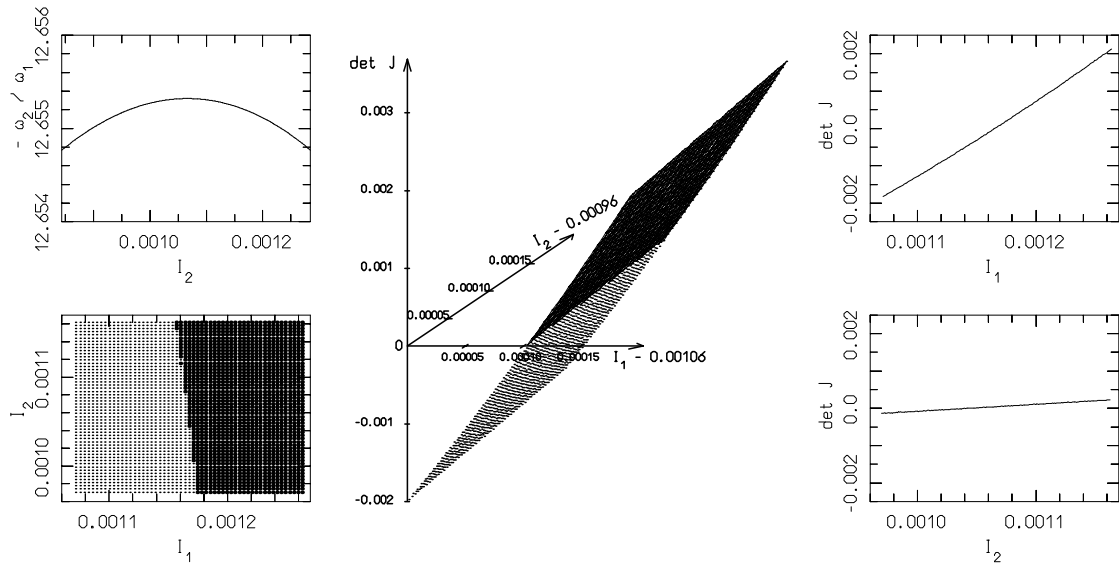
Figure 7: Local study of the Jacobian J of the map associating actions and frequencies. Top–left box: behavior of the ratio of the frequencies corresponding to initial conditions on the line connecting those which generate the invariant tori plotted in Figure 6. Middle picture: 3D plot of det J as a function of the initial values of the actions (the initial values of the angles are always the same as in the maximum point of the picture in the top–left box, i.e. $\varphi_1 = 0.205173$ and $\varphi_2 = 0.244193$). Bottom–left box: grid of the initial values of the actions for which the corresponding points are reported in the middle picture. Both in bottom–left box and in the middle picture, the region corresponding to non-negative [negative, resp.] values of det J have been colored with a darker [lighter] gray. Top–right [bottom–right, resp.] box: section of the function plotted in the middle, after having fixed I_2 [I_1] equal to its medium value in the rectangular grid.

steps. First, we iterate for a fixed number of steps the normalization algorithm by setting to zero the translation vectors $\xi^{(r)}$. Under mild theoretical assumptions, such a partial normalization procedure can still converge to a Hamiltonian in Kolmogorov's normal form related to a vector of angular frequencies ω^* different from ω. Then, using this intermediate Hamiltonian $H \simeq \omega^* \cdot p + \mathcal{O}(p^2)$ as the initial one, we restart a complete standard Kolmogorov's normalization algorithm now including the translation vectors $\xi^{(r)}$ defined in (19). This splitting of the normalization algorithm in two separate steps becomes advantageous if, after the first step, the frequencies ω^* are sufficiently close to ω and, thus, the translation vectors $\xi^{(r)}$ are small enough.

Let us remark that the frequencies ω^*, related to the intermediate Hamiltonian $H \simeq \omega^* \cdot p + \mathcal{O}(p^2)$, depend on the initial translation vector I^* of the canonical transformation (15). Therefore, we try to choose I^* such that the frequency vector ω^* is as close as possible to ω. Thus, we use as a first guess of the "optimal" value of I^* the value of the actions of the initial conditions in the coordinates (I, φ) after the Birkhoff normalization, because those actions should be "nearly" constant and then $(I = I^*, \varphi \in \mathbb{T}^n)$ should be a "good enough" initial approximation of the wanted invariant torus. Therefore, we try to improve our choice of I^*, by approximating numerically the Jacobian matrix $\mathcal{J}_{I^*}$ of the function $\omega^*(I^*)$ and then solving the linear equation $\mathcal{J}_{I^*}(\overline{I} - I^*) = \omega - \omega^*$ in the unknown $\overline{I}$. This value $\overline{I}$ for the initial translation vector is often suitable enough to apply the previous ideas.

We now provide a detailed description of our algorithm. Let us consider as starting point a system of the type described by the Hamiltonian $H^{(\mathrm{II})}$ in (7). Then, let us carry out the following steps.

(a) Perform the canonical transformation $\mathcal{B}$ that realizes the Birkhoff normalization up to a finite degree, as described at point (i) of Section 4.1.

(b) Determine a good initial translation vector $\overline{I}$ by using one step of the following procedure:

(b_1) Let us refer to the initial conditions as (I_0, φ_0); calculate their values in the new coordinates, say $(I_0^*, \varphi_0^*) = \mathcal{B}(I_0, \varphi_0)$. Then, perform the initial translation of the actions, as at point (ii) of Section 4.1, by replacing I^* with I_0^*.

(b_2) Let us perform the Kolmogorov's normalization algorithm up to a fixed R'-th step, as at point (iii) of Section 4.1, starting from $H^{(1)} = H^{(\mathrm{VI})}$, but putting the translation vectors $\xi^{(r)} = 0$, $\forall r = 2, \ldots, R'$. Let us define ω_0^* in such a way that $\omega_0^* \cdot p = \omega \cdot p + f_1^{(0,r+1)}(p)$, with $f_1^{(0,r+1)}$ as obtained at the end of such procedure. R' is a fixed integer parameter that is selected sufficiently large to allow the convergence of the whole algorithm, but also taking into consideration the computational resources available.

(b_3) Repeat point (b_1), by replacing now I^* with $I_0^* + (\delta_1 I_0^*)e_1$, where e_1 is the unit vector in the first axis direction and $\delta_1 I_0^*$ is a carefully chosen scalar coefficient such that $|\delta_1 I_0^*| \ll \|I_0^*\|$. More concretely, in the numerical applications, we have defined $\delta_j I_0^* = I_{0,j}^*/1000 \; \forall \; j = 1, \ldots, n$, where $I_0^* = (I_{0,1}^*, \ldots, I_{0,n}^*)$.

$\qquad \vdots$

(b_{2n+1}) Repeat point (b_1), by replacing now I^* with $I_0^* + (\delta_n I_0^*)e_n$.

(b_{2n+2}) Repeat point (b_2), then define $\delta_n \omega_0^*$ in such a way that $(\omega_0^* + \delta_n \omega_0^*) \cdot p =$

$\omega \cdot p + f_1^{(0,R'+1)}(p)$.

(b_{2n+3}) Let matrix A be such that every j–th column is given by $\delta_j \omega_0^* / \delta_j I_0^* \ \forall \ j = 1, \ldots, n$; therefore, $A \simeq \mathcal{J}_{I_0^*}$. Solve the equation $A(\bar{I} - I^*) = \omega - \omega_0^*$ in the unknown $\bar{I}$.

(c) Perform the translation of the actions as at point (ii) of Section 4.1, replacing I^* with $\bar{I}$.

(d) Let us perform the Kolmogorov's normalization algorithm without translations, as at step (b_2). In what follows we will denote as $\{\mathbf{H}^{(r)}\}_{r=1}^{R'}$, $\{\mathbf{X}_1^{(r)}, \mathbf{X}_2^{(r)}\}_{r=2}^{R'}$ and $\{\mathbf{K}^{(r)}\}_{r=2}^{R'}$ the obtained finite sequences of the Hamiltonians, the generating functions and the canonical transformations, respectively; so that $\mathbf{H}^{(1)} = H^{(\mathrm{VI})}$, $\mathbf{H}^{(r)} = \exp L_{\mathbf{X}_2^{(r)}} \big(\exp L_{\mathbf{X}_1^{(r)}} \mathbf{H}^{(r-1)} \big)$ and $\mathbf{H}^{(r)} = \mathbf{H}^{(1)} \circ \mathbf{K}^{(r)}$, $\forall \ r = 2, \ldots, R'$. Therefore, $\mathbf{K}^{(r)}$ is explicitly given by a formula analogous to (29), by replacing the symbols $\mathcal{K}$ and χ with $\mathbf{K}$ and $\mathbf{X}$, respectively.

(e) Let us perform the standard Kolmogorov's normalization algorithm, as at point (iii) of Section 4.1 (with the translation vectors $\xi^{(r)}$ given by (19)), starting from $H^{(1)} = \mathbf{H}^{(R')}$.

The knowledge of the normal form (and of the normalizing transformations) allows for an explicit integration of the motion. For instance, if we consider the coordinates (X, Y, P_X, P_Y) introduced in Section 2.1 and the action-angle variables (p, q) of the normal form, we have that

$$
\begin{array}{ccc}
(X(0), Y(0), P_X(0), P_Y(0)) & \xrightarrow{\ \big(\mathcal{C}^{(\infty)}\big)^{-1}\ } & (p(0) = 0\,,\, q(0)) \\[2mm]
 & & \downarrow \\[2mm]
(X(t), Y(t), P_X(t), P_Y(t)) & \xleftarrow{\ \mathcal{C}^{(\infty)}\ } & (p(t) = p(0)\,,\, q(t) = q(0) + \omega t)
\end{array}
\qquad , \qquad (30)
$$

with $\mathcal{C}^{(r)} = \mathcal{L} \circ \mathcal{A} \circ \mathcal{B} \circ \mathcal{T} \circ \mathbf{K}^{(R')} \circ \mathcal{K}^{(r)}$, where the canonical transformations $\mathcal{L}$ and $\mathcal{A}$ are defined in Section 2.2, and $\mathcal{B}$, $\mathcal{T}$, $\mathbf{K}^{(R')}$ and $\mathcal{K}^{(r)}$ are determined at points (a), (c), (d) and (e) of the algorithm described above, respectively.

We have checked the implementation by comparing some numerical integrations against the results from the normal form, by means of the scheme (30).

5   Description of the results

In Figure 8, we have reported the results of such a comparison for 588 Achilles. More precisely, we have derived its initial conditions in the RTBP planar model from a spherical projection of the spatial coordinates. Then we have numerically calculated the corresponding frequencies of motion $\omega = (\omega_1, \omega_2)$ by using the frequency analysis method. Afterwards, we have carried out the algorithm constructing the invariant torus corresponding to ω by performing both the Kolmogorov's normalization at points (d) and (e) up to the step $r = R' = 20$. A software package, specially designed for the algebraic manipulation, allowed us to produce the expansions of the functions defined by the algorithm. The particular choice in the degree of the Kolmogorov normal form (20-th order) is due to limitations on both software and hardware resources available to us, but it is
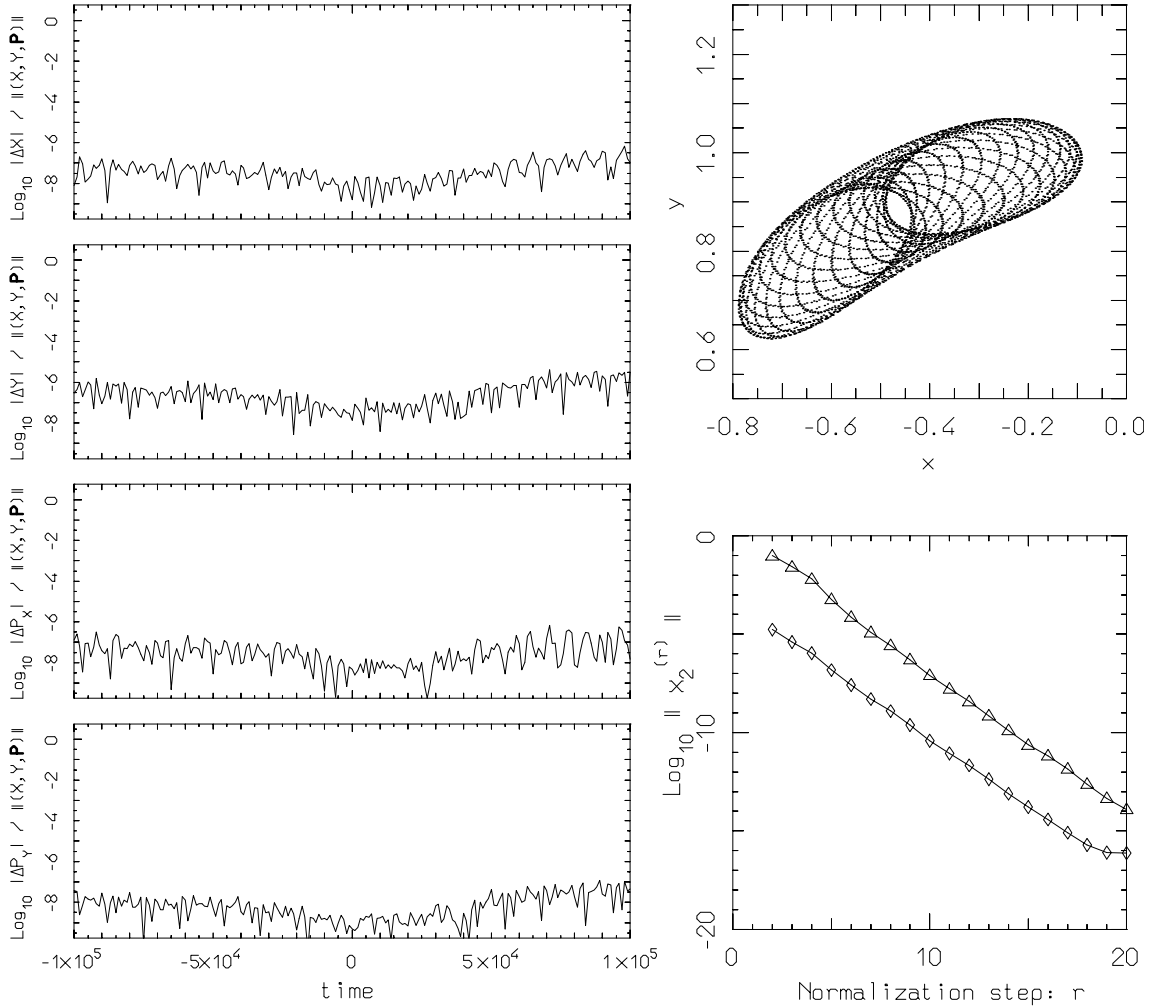
Figure 8: Test on the reliability of the construction of the Kolmogorov's normal form on the planar RTBP for the asteroid 588 Achilles. On the left: time dependency of the relative differences between a numerical integration and the semi-analytic one, based on an approximation of the scheme (30) (see the text for more details). Top-right box: projection of the invariant torus in the (x, y) coordinates. Bottom-right box: behavior of the norm of the generating functions as a function of the normalization step; more precisely, the symbols $\triangle$ [$\lozenge$, resp.] refer to the norm of the generating functions $\mathbf{X}_2$ [χ_2] defined during the Kolmogorov's normalization without [with] translations, as described at point (d) [(e)] of Section 4.3.
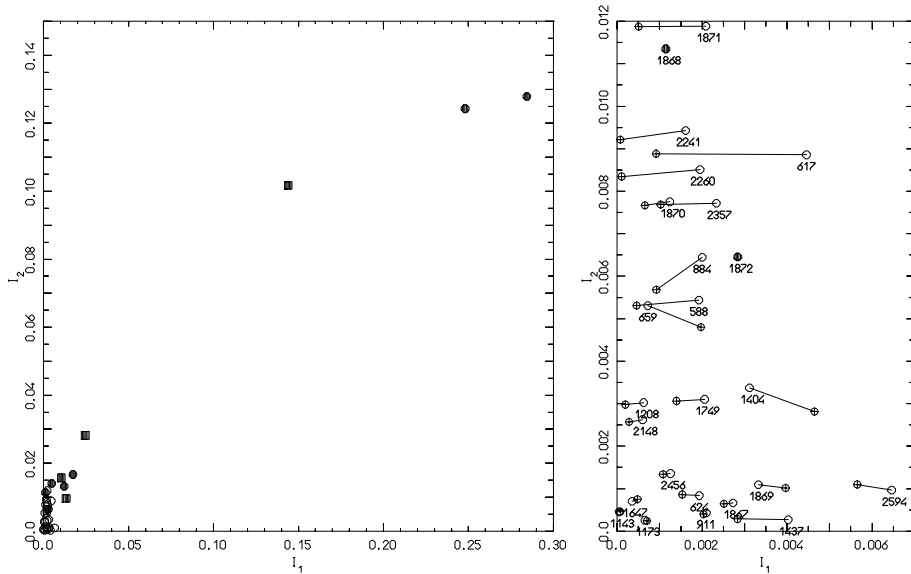
Figure 9: Summary of the results of the algorithm constructing invariant tori. In correspondence with the values of the actions (I_1, I_2) related to the initial conditions (expressed in the coordinates (I, φ) previous to the Birkhoff normalization), we have used the symbol ■ when the orbit is chaotic, ● if the algorithm does not converge and ○ if it does. The figure on the right is an enlargement of the one in the left. In addition, in the right figure, below every symbol, we show the catalog number of the corresponding asteroid. Moreover, for each case where the algorithm converges, the corresponding initial translation vector $(\overline{I}_1, \overline{I}_2)$ has been indicated with the symbol $\oplus$.

already enough for our purposes. Thus, it has been possible to approximate the motion in a semi-analytic way by using the normal form and the scheme (30), where we have replaced $\mathcal{C}^{(\infty)}$ with $\mathcal{C}^{(20)}$. Finally, we have compared this semi-analytic integration of the equations of motion with a numerical one. The behavior of the relative difference $\Delta(X(t), Y(t), \mathbf{P}(t))/\|(X(t), Y(t), \mathbf{P}(t))\|$ (where, for short, $\mathbf{P}$ means P_X, P_Y) is plotted in the left column of Figure 8, on the time interval $[-10^5, 10^5]$, whose width corresponds to about 0.4 My. The agreement between the results of the two methods is excellent. Indeed, in terms of the synodical coordinates (x, y), the absolute difference between the values of each coordinate as calculated by the two different methods stays within 5.3×10^{-7} (which is equivalent to an error of about 10^{-7} A.U., comparable to the current uncertainty of the observations). In the top-right box of Figure 8, we have projected the invariant torus on the synodical coordinates (x, y). We can appreciate that the invariant torus extends also quite far away from the equilibrium point (compare with Figure 1) and the area filled by its projection is not negligible at all with respect to the region described by the initial conditions of the asteroids (look at Figure 2). Moreover, in the bottom-right box of Figure 8, we reported the norm (given by formula (31)) of the generating functions. We can appreciate a sharp geometrical decreasing of the norms as a function of the normalization step for the generating functions defined by Kolmogorov's normalizations with and without the translations.

We have applied this procedure for the first 34 Trojan asteroids of the catalog. The initial conditions in the RTBP with spherical projection in the plane $z = 0$, give rise to orbits which either have close encounters with Jupiter or are strongly chaotic in four cases (that are 1172 Aneas, 1583 Antilochus, 1873 Agenor and 2223 Sarpedon). For what concerns the remaining 30 asteroids, the corresponding motions look quasi-periodic according to the frequency analysis method. Hence, it has been possible to apply the algorithm to construct the corresponding invariant torus. The algorithm does not work properly for 7 other asteroids: 1868 Thersites, 1872 Helenos, 2146 Stentor, 2207 Antenor, 2363 Cebriones, 2674 Pandarus and 2759 Idomeneus. For all the remaining cases, the sequences of the norms of the generating functions $\mathbf{X}_2^{(r)}$ and $\chi_2^{(r)}$ (defined at point (d) and (e) of Section 4.3, respectively) show a very regular geometrically decreasing behavior similar to the one in the bottom-right box of Figure 8. Therefore, the algorithm is clearly convergent for all these 23 asteroids.

The results are visualized in Figure 9, by referring to the same plane (I_1, I_2), used in Section 3 to numerically study the stability region close to the equilibrium point. By comparing the picture on the left of Figure 9 with Figure 5, we immediately remark that our algorithm seem to be convergent every time that the initial values of the actions are located in the "usual" stability region (with the possible exception of 1868 Thersites and 1872 Helenos, which look very close to a resonant zone). On the other hand, the algorithm does not work when the initial actions are too big.

The main results obtained are summarized in Table 1. In the fourth and fifth column of this table, we have reported the decimal logarithm of the ratios $\frac{\|\mathbf{X}_2^{(20)}\|}{\|\mathbf{X}_2^{(2)}\|}$ and $\frac{\|\chi_2^{(20)}\|}{\|\chi_2^{(2)}\|}$, respectively. Of course, the smaller these ratios are the faster the convergence of the algorithm is. The initial translation vectors $\overline{I}$ (determined according to the point (b) of Section 4.3) are reported in the third column. Let us recall that the size of the perturbation is essentially ruled by the translation vector, as discussed at point (ii) of Section 4.1. Comparing the third column with the fourth and the fifth ones, one can appreciate that the bigger $\overline{I}$ is, the slower the convergence of the algorithm. Note that the distance in the direction I_1 has a larger weight compared to I_2.

In the last column we report the maximum for $t \in [-10^5, 10^5]$ of the relative difference $\Delta(X(t), Y(t), \mathbf{P}(t))/\|(X(t), Y(t), \mathbf{P}(t))\|$ between the values of $(X, Y, \mathbf{P})$ calculated by the numerical integration of the RTBP and those given by the semi-analytic one, based on the scheme (30). Let us remark that the relative difference is always nearly aligned in the direction of the second component (in terms of the polar coordinates, this corresponds to the angular variable). The agreement between the two methods is not always as good as in the case of 588 Achilles represented in Figure 8. Indeed, (the second component of) the maximum of the relative difference ranges between 8×10^{-7} and 2×10^{-2}.

The behavior of $\mathrm{Max}_{t \in [-10^5, 10^5]}[\|\Delta(X(t), Y(t), \mathbf{P}(t))\|/\|(X(t), Y(t), \mathbf{P}(t))\|]$ as a function of either $\overline{I}_1$ or $\overline{I}_1/\overline{I}_2$ is rather regular, as shown in Figure 10. The data corresponding to the asteroids reported in Table 1 are mainly located close to the diagonal of the two pictures and, sometimes, they are quite well grouped together (especially in the right plot). The agreement between the two methods is obviously good when the translation vector is small, but, rather surprisingly, the cases with low perturbation (or, equivalently,

Table 1: Main results of the algorithm constructing the invariant tori related to some of the Trojan asteroids.

| asteroid number	(ω_1, ω_2)	$(\overline{I}_1, \overline{I}_2)$	$\mathrm{Lg}_{10} \frac{\|\mathbf{X}_2^{(20)}\|}{\|\mathbf{X}_2^{(2)}\|}$	$\mathrm{Lg}_{10} \frac{\|\chi_2^{(20)}\|}{\|\chi_2^{(2)}\|}$	$\mathrm{Max}\, \frac{\Delta(X,Y,\mathbf{P})}{\|(X,Y,\mathbf{P})\|}$
588	$\begin{pmatrix} -0.080715474188664579, \\ 0.99675295177491230 \end{pmatrix}$	$\begin{pmatrix} 4.5735621245671771 \cdot 10^{-4}, \\ 5.3079239711385654 \cdot 10^{-3} \end{pmatrix}$	-12.1	-11.3	$\begin{pmatrix} 0.7, 4.1, \\ 0.7, 0.1 \end{pmatrix} \cdot 10^{-6}$
617	$\begin{pmatrix} -0.080618182744496350, \\ 0.99673748443899368 \end{pmatrix}$	$\begin{pmatrix} 9.1746188112155165 \cdot 10^{-4}, \\ 8.8835072759784871 \cdot 10^{-3} \end{pmatrix}$	-8.3	-8.1	$\begin{pmatrix} 0.1, 1.9, \\ 0.3, .04 \end{pmatrix} \cdot 10^{-5}$
624	$\begin{pmatrix} -0.078748184482131778, \\ 0.99654000611164795 \end{pmatrix}$	$\begin{pmatrix} 1.5329854933817534 \cdot 10^{-3}, \\ 8.6242199419992414 \cdot 10^{-4} \end{pmatrix}$	-12.0	-11.8	$\begin{pmatrix} .08, 4.0, \\ 0.1, .02 \end{pmatrix} \cdot 10^{-4}$
659	$\begin{pmatrix} -0.078689625901293248, \\ 0.99654350614361831 \end{pmatrix}$	$\begin{pmatrix} 1.9747523334567290 \cdot 10^{-3}, \\ 4.7997474480390070 \cdot 10^{-3} \end{pmatrix}$	-9.4	-7.0	$\begin{pmatrix} 0.5, 8.4, \\ 0.9, 0.2 \end{pmatrix} \cdot 10^{-5}$
884	$\begin{pmatrix} -0.080192594354172447, \\ 0.99669396075437633 \end{pmatrix}$	$\begin{pmatrix} 9.2304803423234698 \cdot 10^{-4}, \\ 5.6786282923325711 \cdot 10^{-3} \end{pmatrix}$	-11.7	-11.5	$\begin{pmatrix} 0.2, 1.7, \\ 0.3, .04 \end{pmatrix} \cdot 10^{-5}$
911	$\begin{pmatrix} -0.078023449274368356, \\ 0.99646166210736797 \end{pmatrix}$	$\begin{pmatrix} 2.0339468870637896 \cdot 10^{-3}, \\ 4.0062233825115912 \cdot 10^{-4} \end{pmatrix}$	-10.8	-10.5	$\begin{pmatrix} 0.1, 4.7, \\ .08, .02 \end{pmatrix} \cdot 10^{-4}$
1143	$\begin{pmatrix} -0.080453760255799589, \\ 0.99675168085465859 \end{pmatrix}$	$\begin{pmatrix} 7.1640448838141430 \cdot 10^{-5}, \\ 4.5625478370349924 \cdot 10^{-4} \end{pmatrix}$	-24.8	-18.8	$\begin{pmatrix} 2.4, 8.0, \\ 2.1, 0.2 \end{pmatrix} \cdot 10^{-6}$
1173	$\begin{pmatrix} -0.079687873098300360, \\ 0.99665301540279361 \end{pmatrix}$	$\begin{pmatrix} 7.0262988406317041 \cdot 10^{-4}, \\ 2.4071855168768738 \cdot 10^{-4} \end{pmatrix}$	-16.6	-13.1	$\begin{pmatrix} .04, 1.2, \\ .07, .007 \end{pmatrix} \cdot 10^{-4}$
1208	$\begin{pmatrix} -0.080696004278632952, \\ 0.99676302348820989 \end{pmatrix}$	$\begin{pmatrix} 1.9125277447561861 \cdot 10^{-4}, \\ 2.9778876846574278 \cdot 10^{-3} \end{pmatrix}$	-16.2	-11.4	$\begin{pmatrix} 0.9, 7.8, \\ 1.4, 0.2 \end{pmatrix} \cdot 10^{-6}$
1404	$\begin{pmatrix} -0.074339814942229479, \\ 0.99619812988465195 \end{pmatrix}$	$\begin{pmatrix} 4.6470852511240716 \cdot 10^{-3}, \\ 2.8117200051766301 \cdot 10^{-3} \end{pmatrix}$	-5.6	-5.5	$\begin{pmatrix} 0.3, 4.8, \\ 0.3, .09 \end{pmatrix} \cdot 10^{-3}$
1437	$\begin{pmatrix} -0.076892743880210571, \\ 0.99635020293565268 \end{pmatrix}$	$\begin{pmatrix} 2.8363044344569010 \cdot 10^{-3}, \\ 2.8746815778802861 \cdot 10^{-4} \end{pmatrix}$	-7.5	-6.4	$\begin{pmatrix} .03, 1.6, \\ .03, .004 \end{pmatrix} \cdot 10^{-3}$
1647	$\begin{pmatrix} -0.080027652156843390, \\ 0.99669299882105700 \end{pmatrix}$	$\begin{pmatrix} 4.8053543816242646 \cdot 10^{-4}, \\ 7.5059131290292904 \cdot 10^{-4} \end{pmatrix}$	-18.0	-13.4	$\begin{pmatrix} 0.2, 2.2, \\ 0.1, .03 \end{pmatrix} \cdot 10^{-5}$
1749	$\begin{pmatrix} -0.079233437316304542, \\ 0.99659266795195256 \end{pmatrix}$	$\begin{pmatrix} 1.3960082696097675 \cdot 10^{-3}, \\ 3.0645766576859793 \cdot 10^{-3} \end{pmatrix}$	-11.8	-11.4	$\begin{pmatrix} 0.3, 3.5, \\ 0.3, .07 \end{pmatrix} \cdot 10^{-5}$
1867	$\begin{pmatrix} -0.077400216491750912, \\ 0.99640034798208466 \end{pmatrix}$	$\begin{pmatrix} 2.5125755624158183 \cdot 10^{-3}, \\ 6.4564726053964829 \cdot 10^{-4} \end{pmatrix}$	-9.1	-7.3	$\begin{pmatrix} .05, 1.1, \\ .09, .005 \end{pmatrix} \cdot 10^{-4}$
1869	$\begin{pmatrix} -0.075273368358587736, \\ 0.99622553356358334 \end{pmatrix}$	$\begin{pmatrix} 3.9658962836038826 \cdot 10^{-3}, \\ 1.0138420157461863 \cdot 10^{-3} \end{pmatrix}$	-6.9	-7.0	$\begin{pmatrix} .07, 3.1, \\ .08, .002 \end{pmatrix} \cdot 10^{-4}$
1870	$\begin{pmatrix} -0.080795233402109923, \\ 0.99675584255254235 \end{pmatrix}$	$\begin{pmatrix} 6.5354209594490167 \cdot 10^{-4}, \\ 7.6674696509944230 \cdot 10^{-3} \end{pmatrix}$	-9.1	-8.6	$\begin{pmatrix} 1.0, 5.4, \\ 0.9, 0.3 \end{pmatrix} \cdot 10^{-6}$
1871	$\begin{pmatrix} -0.081514040787185243, \\ 0.99682673629125285 \end{pmatrix}$	$\begin{pmatrix} 5.0828198584491674 \cdot 10^{-4}, \\ 1.1874638620374238 \cdot 10^{-2} \end{pmatrix}$	-5.8	-5.5	$\begin{pmatrix} 0.3, 1.8, \\ 0.7, .05 \end{pmatrix} \cdot 10^{-3}$
2148	$\begin{pmatrix} -0.080533074925310380, \\ 0.99674515743171077 \end{pmatrix}$	$\begin{pmatrix} 2.7971788895957324 \cdot 10^{-4}, \\ 2.5682028661620252 \cdot 10^{-3} \end{pmatrix}$	-16.4	-12.6	$\begin{pmatrix} 0.9, 7.0, \\ 1.3, 0.2 \end{pmatrix} \cdot 10^{-6}$
2241	$\begin{pmatrix} -0.081707303284590957, \\ 0.99685130480612028 \end{pmatrix}$	$\begin{pmatrix} 7.3644442596587732 \cdot 10^{-5}, \\ 9.2156409035582809 \cdot 10^{-3} \end{pmatrix}$	-10.1	-7.8	$\begin{pmatrix} 1.0, 8.0, \\ 2.1, 0.2 \end{pmatrix} \cdot 10^{-7}$
2260	$\begin{pmatrix} -0.081556086303685743, \\ 0.99683754696145255 \end{pmatrix}$	$\begin{pmatrix} 1.0272079815504267 \cdot 10^{-4}, \\ 8.3465843575113198 \cdot 10^{-3} \end{pmatrix}$	-11.3	-9.1	$\begin{pmatrix} 0.2, 1.6, \\ 0.3, .03 \end{pmatrix} \cdot 10^{-6}$
2357	$\begin{pmatrix} -0.080330839991193073, \\ 0.99670820475542277 \end{pmatrix}$	$\begin{pmatrix} 1.0216317484861338 \cdot 10^{-3}, \\ 7.6859257344373544 \cdot 10^{-3} \end{pmatrix}$	-10.0	-9.1	$\begin{pmatrix} 0.6, 6.6, \\ 1.0, 0.3 \end{pmatrix} \cdot 10^{-6}$
2456	$\begin{pmatrix} -0.079390776282647166, \\ 0.99661226620203403 \end{pmatrix}$	$\begin{pmatrix} 1.0796571731783104 \cdot 10^{-3}, \\ 1.3388711955805834 \cdot 10^{-3} \end{pmatrix}$	-13.7	-11.7	$\begin{pmatrix} .07, 1.5, \\ .07, .02 \end{pmatrix} \cdot 10^{-4}$
2594	$\begin{pmatrix} -0.072399117763879486, \\ 0.99605155197123274 \end{pmatrix}$	$\begin{pmatrix} 5.6531551656997595 \cdot 10^{-3}, \\ 1.0973030849600765 \cdot 10^{-3} \end{pmatrix}$	-5.4	-4.9	$\begin{pmatrix} .07, 1.7, \\ 0.1, .03 \end{pmatrix} \cdot 10^{-2}$
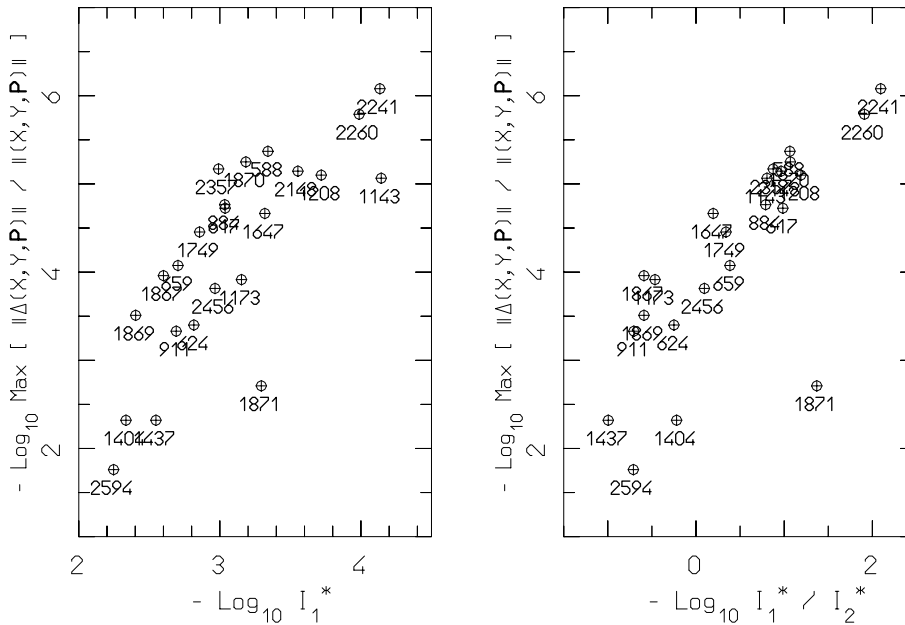
Figure 10: The maximum of the relative difference on $\|(X, Y, \mathbf{P})\|$ as a function of the first component of the initial translation (picture on the left) and of the ratio of the two components (on the right) for all the asteroids for which our algorithm ends successfully.

with a fast convergence to zero of the generating functions) are not those corresponding to the best results: we can see it, for instance, by comparing the rows related to 1173 Anchises and 1647 Menelaus with 2241 Alcathous. In general, when $\overline{I}_2 \gg \overline{I}_1$ (i.e. on the right part of the pictures in Figure 10), we have an excellent agreement between the two methods. Indeed, there is only one of such cases (i.e. 1871 Astyanax, which looks very far from the diagonal in Figure 10) where the maximum of the relative difference is larger than 2×10^{-5}; but the initial conditions of that asteroid are quite far from the equilibrium point and in that case we remarked that, by calculating slightly smaller expansions of the functions, the final results are clearly worse, therefore, we expect that the agreement can be improved by increasing the size of the expansions. Note that the size of the expansions is not only determined by the final number of the performed steps of the algorithm. Indeed, there are many parameters ruling the truncations of Hamiltonians and canonical transformations, that will be described in the next section.

The agreement between the semi-analytic integration and the numerical one progressively deteriorates when the value of either $\overline{I}_1$ or $\overline{I}_1/\overline{I}_2$ increases, up to the worst case of 2594 Acamas. Moreover, we have seen that using slightly smaller expansions of the functions to calculate the parametric equations of the final invariant tori, the difference between the two methods of integration remains approximately the same for all the asteroids except for the above discussed case of 1871 Astyanax (in most of the cases the agreement is even better with smaller expansions). These facts bring us to conclude that the main limitation on the precision of the semi-analytic integration should be due to the accumulation of the numerical errors in the calculation of the truncated series approximating the canonical transformations. The size of this error seems to be mainly ruled by

the value of $\overline{I}_1$.

6   Details on the computer–assisted proof

The proof is done for a high order expansion of the Hamiltonian. To avoid the control of the estimates for all the canonical transformations of Section 4, we will start the computer–assisted proofs from point (d) of the algorithm described in Section 4.3. The last column of Table 1 contains also an estimate of the size of the modification introduced by working on a truncated expansion of the RTBP instead of the true RTBP given by (1). Note that for asteroids whose value of $\overline{I}_1$ is not too big, the differences due to the change of models are not physically relevant.

We will introduce a further simplification. In order to prove that an orbit cannot diffuse anywhere in the phase space, one should ensure that there is a topological confinement. The basic element to carry on this "trapping strategy" is the proof of the existence of families of invariant tori which are close to the initial conditions and have a fixed (Diophantine) ratio of the frequencies (ω_1, ω_2). Then, the two final trapping tori are given by the intersection of the fixed level of energy with two "good" families that are selected by trial and error (see [LG00]). In this paper, we will simply prove the existence of some families of invariant tori close to the initial conditions of some asteroids, without completing the trapping method.

Let us now precisely state which is the starting point of our computer–assisted proof. We first did all the canonical transformations described in Section 2. Then, we performed the Birkhoff normalization as described at point (i) of Section 4.1, by truncating the Hamiltonian up to degree 60 in the actions I. Afterwards, we did the initial translation of the actions as at point (ii) of Section 4.1, where the value of the vector $\overline{I}$ for each asteroid is reported in the third column of Table 1. In this case, we truncated the Hamiltonian up to degree 20 in the actions p and to degree 42 in the angles q. Thus, we derived 23 different initial Hamiltonians (that we indicate with the symbol $\mathcal{H}^{(n_\#)}$) and each of them is related to the asteroid with catalog number $n_\#$. For each of them, by adapting the technique used in [LG00], we tried to prove the existence of a family of tori with frequencies very close to the corresponding ones in the second column of Table 1. In the following, we describe such modifications.

Let us first introduce some notations. If $v \in \mathbb{R}^n$, we denote $|v| = \sum_{j=1}^{n} |v_j|$. Also, we write the expansion of a generic function $g \in \mathcal{P}_{l,K}$, with multi-index notation, as $g(p,q) = \sum_{|j|=l} \sum_{|k| \leq K} [c_{jk} p^j \cos(k \cdot q) + d_{jk} p^j \sin(k \cdot q)]$. Then we introduce the norm

$$\|g\| = \sum_{|j|=l} \sum_{|k| \leq K} \big[|c_{jk}| + |d_{jk}| \big] . \tag{31}$$

We need estimates for the norms of the functions $\mathbf{f}_l^{(r,s)}$ and $f_l^{(r,s)}$ appearing in

$$\mathbf{H}^{(r)}(p,q) = \omega \cdot p + \sum_{s \geq 0} \sum_{l \geq 0} \mathbf{f}_l^{(r,s)}(p,q) , \tag{32}$$

and (25), respectively; where the sequences of Hamiltonians $\{\mathbf{H}^{(r)}\}_{r=1}^{R'}$ and $\{H^{(r)}\}_{r=1}^{R''}$ are defined as at points (d) and (e) of Section 4.3, starting from $\mathbf{H}^{(1)} = \mathcal{H}^{(n_\#)}$ and from $H^{(1)} = \mathbf{H}^{(R')}$. More precisely, we select a couple of positive integers R' and R'' (to fix the ideas, in the following we will assume $R' = 24$ and $R'' = 2048$); then, we look for a positive constant E and four finite sequences $\{\mathbf{e}_r\}_{r=1}^{R'}$, $\{\mathbf{z}_r\}_{r=1}^{R'}$, $\{\varepsilon_r\}_{r=1}^{R''}$ and $\{\zeta_r\}_{r=1}^{R''}$ of positive real numbers such that

$$
\begin{aligned}
\left\| \mathbf{f}_l^{(r,s)} \right\| &\leq \mathbf{e}_r^s E \, \mathbf{z}_r^l && \text{for } 1 \leq r \leq R', \ s \geq 0, \ l \gtrless 0 \\
\left\| f_l^{(r,s)} \right\| &\leq \varepsilon_r^s E \, \zeta_r^l && \text{for } 1 \leq r \leq R'', \ s \geq 0, \ l \gtrless 0
\end{aligned}
\tag{33}
$$

The estimates are obtained as follows:

(a) Estimate of the generating functions $\mathbf{X}_1^{(2)}$, $\mathbf{X}_2^{(2)}$, ..., $\mathbf{X}_1^{(R')}$, $\mathbf{X}_2^{(R')}$, $\chi_1^{(2)}$, $\chi_2^{(2)}$, ..., $\chi_1^{(R'')}$, $\chi_2^{(R'')}$, and of all the intermediate functions necessary to evaluate the previous ones. This is obtained through a preliminary explicit calculation (by following the prescriptions given in Section 4, but using intervalar arithmetic, see, e.g., [KSW96] and [SWW00]) of all the coefficients appearing in the expansions of the functions $\mathbf{f}_l^{(r,s)}$ and $f_l^{(r,s)}$ with $0 \leq l \leq 20$, $1 \leq r \leq R'$ and $0 \leq s \leq R' + 1$. Then, we used a scheme of iterative estimates analogous to that described in Section 4.1.1 of [LG00]. We just introduced a few obvious changes because here we have to estimate also the terms $\mathbf{f}_l^{(r,s)}$ of the Hamiltonians $\mathbf{H}^{(r)}$ generated by the preliminary Kolmogorov's normalization algorithm without translations. Following such a procedure, we obtain explicit upper bounds for the functions $\mathbf{f}_l^{(r',s)}$, $\mathbf{X}_1^{(2)}$, $\mathbf{X}_2^{(2)}$, ..., $\mathbf{X}_1^{(R')}$, $\mathbf{X}_2^{(R')}$, and $f_l^{(r'',s)}$, $\chi_1^{(2)}$, $\chi_2^{(2)}$, ..., $\chi_1^{(R'')}$, $\chi_2^{(R'')}$, with $0 \leq l \leq 20$, $1 \leq r' \leq R'$, $1 \leq r'' \leq R''$ and $0 \leq s \leq R'' + 1$.

(b) Derivation of the upper bounds (33) on the infinite sequence of terms appearing in the expansions (32) and (25). Here, we have found convenient to start by defining

$$
\mathbf{e}_1 = \max_{j=1,2} \left\{ \left\| \frac{\partial \mathbf{X}^{(2)}}{\partial q_j} \right\| \right\}, \qquad \mathbf{z}_1 = \max_{j=1,2} \left\{ \frac{1}{\overline{I}_j} \right\}.
\tag{34}
$$

Then, we select E as the minimum value such that the first inequality in (33) is satisfied for $r = 1$ (let us recall that we only have to check a finite number of inequalities, because the Hamiltonian $\mathbf{H}^{(1)}$ is truncated in such a way that $\mathbf{f}_l^{(1,s)} = 0$ if $l > 20$ or $s > 21$). We obtained the values of the terms appearing in the finite sequences $\{\varepsilon_r\}_{r=1}^{R''}$ and $\{\zeta_r\}_{r=1}^{R''}$ by applying iteratively the formulæ (46) and (48) of [LG00], starting from $\varepsilon_1 = \mathbf{e}_{R'}$ and $\zeta_1 = \mathbf{z}_{R'}$; while $\{\mathbf{e}_r\}_{r=1}^{R'}$ and $\{\mathbf{z}_r\}_{r=1}^{R'}$ are analogously derived, by replacing in (46) and (48) of [LG00] the symbols ε, ζ with $\mathbf{e}$, $\mathbf{z}$ and the quantities $\mathcal{G}_{11}^{(r)}$, $\mathcal{G}_{12}^{(r)}$, $\mathcal{G}_{21}^{(r)}$ and $\mathcal{G}_{22}^{(r)}$ with $\max_j \left\{ \left\| \partial \mathbf{X}_1^{(r)}/\partial q_j \right\| \right\}$, 0, $\max_j \left\{ \left\| \partial \mathbf{X}_2^{(r)}/\partial q_j \right\| \right\}$ and $\max_j \left\{ \left\| \partial \mathbf{X}_2^{(r)}/\partial p_j \right\| \right\}$, respectively.

Let us now discuss the results obtained. For three asteroids (namely, 1143 Odysseus, 1173 Anchises and 1647 Menelaus) we have found that the functions generated by the

Table 2: Summary of the upper bounds obtained through a computer–assisted proof. The ratio $-\omega_1/\omega_2$ is given by its expansion in continued fractions.

code num.	$-\omega_1/\omega_2$	Range of ω_1	ε_{2048}	E	ζ_{2048}
1143	$[0,12,2,1,1,3,12,1,4,64,2,\bar{1}]$	$-10^{-10} \leq 1 + \frac{\omega_1}{0.080453760256} \leq 10^{-10}$	0.64	8.7×10^{-4}	1.7×10^{5}
1173	$[0,12,1,1,35,2,2,1,2,133,11,\bar{1}]$	$-10^{-10} \leq 1 + \frac{\omega_1}{0.079687873098} \leq 10^{-10}$	0.77	3.0×10^{-4}	5.1×10^{4}
1647	$[0,12,2,4,1,43,5,2,\bar{1}]$	$-10^{-10} \leq 1 + \frac{\omega_1}{0.080027652157} \leq 10^{-10}$	0.75	1.8×10^{-3}	2.6×10^{4}

algorithm satisfy the estimates in (33) up to $R'' = 2048$ with the final values of ε_{2048}, E and ζ_{2048} reported in Table 2, when the frequencies ω_1 and ω_2 are subject to the restrictions described both in the second and third column of Table 2. For these three asteroids, we can apply Theorem 2 in [LG00] (proved in [Loc01]), because the threshold value ε^* calculated as in the statement of that theorem is always grater than ε_{2048} (i.e. $\varepsilon^* \simeq 0.85$ in all the three cases). Therefore, we can claim the following

Theorem: *Let us consider the three different conservative dynamical systems related to the Hamiltonians $\mathcal{H}^{(n_\#)}$ (defined at the beginning of the present section), where the catalog number $n_\#$ can be equal to 1143, 1173 or 1647. They admit one family of invariant tori each. These three families of tori are such that the fixed ratio of the frequencies ω_1/ω_2 and the range of ω_1 have the values reported in the second and in the third column of Table 2, respectively.*

Let us recall that the possibility of applying the KAM–type Theorem 2 in [LG00] strongly depends both on the number of steps for which we explicitly compute the functions generated by the algorithm (i.e. R') and on the number of times we iterate the estimates (i.e. R''), with the help of a computer (see the related discussion in [CGL00]). The choice of these parameters (i.e. $R' = 24$ and $R'' = 2048$) had to take into account the limits imposed by the computing resources available to us, but it has been suitable enough for our purposes.

When we compare the results in Table 2 with Figure 9, it is clear that the computer-assisted proof has been successful for the closest asteroids to the equilibrium point.

What about the remaining asteroids? We think that a few technical modifications of the iterative estimates should be enough to prove the existence of invariant tori close to the orbits of some asteroids, that are near the equilibrium point (namely, 624 Hektor, 1208 Troilus, 2148 Epeios and 2456 Palamedes). The idea is the following: in the cases quoted above, the method fails because, from the iterative formulas (46) and (48) of [LG00], it follows that $\varepsilon_r \geq \exp(\sum_{j=2}^{r} 2/j^3)\varepsilon_1$, even when the generating functions are very small. Such a problem can be overcome, by just skipping a few steps of the standard Kolmogorov's normalization (i.e. the one including the translations) and by restarting the algorithm from a $r = \bar{r}$ such that

$$\varepsilon_1 \simeq \left[\bar{r}^2 \left(\mathcal{G}_{11}^{(\bar{r})} + \mathcal{G}_{12}^{(\bar{r})} \right) \zeta_{\bar{r}-1} \right]^{1/\bar{r}}$$

and

$$\varepsilon_1 \simeq \left[\bar{r}^2 \max \left\{ \mathcal{G}_{21}^{(\bar{r})} , \, 2\bar{r}\mathcal{G}_{22}^{(\bar{r})} \right\} \right]^{1/\bar{r}} .$$

On the other hand, we remarked that even the sequence of upper bounds generated by the iteration of the estimates in Section 4.1.1 of [LG00] (which is previous to the calculation of the sequences $\{\varepsilon_r\}_{r=1}^{R''}$ and $\{\zeta_r\}_{r=1}^{R''}$, that introduces a further worsening effect) looks clearly divergent for the following asteroids: 2260 Neoptolemus, 1870 Glaukos, 884 Priamus, 659 Nestor, 1404 Ajax, 1869 Philoctetes. A rigorous proof of existence of tori near to the orbits of these objects, or those located even farther from the equilibrium point, looks beyond the limits of our scheme of computer–assisted proof. There are four other asteroids (namely, 588 Achilles, 911 Agamemnon, 1437 Diomedes, 1867 Deiphobus) for which our approach might be successful, but this should require some technical improvements other than those suggested here.

Let us recall that we have not rigorously proved the stability of the motion of any asteroid, because we did not try to ensure the confinement of the orbit by completing the "trapping strategy". Since the effects of the gravitational attraction exerted by Saturn (and by the other major planets) do strongly change in time the values of the vector $\overline{I}$ related to the various asteroids, we consider that our previous analysis is more interesting than having produced a complete result of stability related to some particular initial conditions. In fact, we think that our discussion shows clearly enough the capabilities and the limits of these techniques.

7 Conclusions

In this paper, we have studied the problem of the stability of the Trojan asteroids in the context of the planar RTBP. The basic techniques that we have used are:

1. The frequency analysis method: to compute the fundamental frequencies for a set of Trojans and to investigate the global dynamics in a neighbourhood of the Lagrangian points.

2. A variation of the Kolmogorov's normalization algorithm: to construct an invariant KAM torus for each pair of frequencies.

The frequency analysis method helped us to highlight some interesting features of the planar RTBP related to our problem. Indeed, the numerical study near the equilateral points in the action-angle variables (I, φ) defined in Section 2.2 reveals that the extension of the stability region with respect to the actions, I, can become much larger if the angles, φ, have some particular values. This fact is very unpleasant if one is interested in a perturbative approach, because the coordinates (I, φ) are the usual starting point for applying Birkhoff or KAM theory and the size of the perturbation is (roughly) proportional to the norm of the actions. Moreover, the frequency analysis has revealed a further difficulty for such theoretical approaches, i.e. the existence of a manifold (not far from the equilibrium point) where the correspondence between actions and frequencies is degenerate.

The variation in the Kolmogorov's normalization algorithm is needed due to the fact that we want to construct invariant tori at some distance from the equilibrium point. The translations of the actions involved in the algorithm are the main source of numerical instability and may prevent the procedure to be convergent. To solve this inconvenient,

first we have constructed an intermediate object (a "quasi-invariant" torus) without using the translations of the actions and, then, this quasi-invariant torus is used as the starting point of a new Kolmogorov's normalization, targeting now the final torus. To implement this strategy in an efficient way, we use a procedure that selects an intermediate torus that is close to the final one. We think that the main source of improvement in the analytic part of this work is due to this new strategy. In fact, our algorithm succeeded in 23 over the 30 cases considered. This corresponds to improve the area of success by a factor close to 100 compared to previous methods (see Table 1 of both [GS97] and [SD00]).

We have also seen that our reformulation of the Kolmogorov's normalization algorithm can be translated in a computer–assisted proof of existence of invariant tori. We successfully used this technique for the three closest asteroids to the equilibrium point.

Finally, let us remark that, even though we have dealt with an application to a classical problem of Celestial Mechanics, systems close to an elliptic equilibrium point actually occur in many problems of physics and chemistry. Since our new perturbative approach try to overcome some difficulties that are peculiar to neighborhoods of elliptic points and the strategy used here does not exploit in a particular way the features of our actual problem, we believe that our procedure can have interesting applications in many different fields.

Acknowledgments

References

References

[AKN88]   V.I. Arnold, V.V. Kozlov, and A.I. Neishtadt. *Dynamical Systems III*, volume 3 of *Encyclopaedia Math. Sci.* Springer, Berlin, 1988.

[Arn63]   V.I. Arnold. Proof of A.N. Kolmogorov's theorem on the preservation of quasi-periodic motions under small perturbations of the Hamiltonian. *Russian Math. Surveys*, 18(5):9–36, 1963.

[Arn64]   V.I. Arnold. Instability of dynamical systems with several degrees of freedom. *Soviet Math. Dokl.*, 5:581–585, 1964.

[Bow]   E. Bowell. The asteroid orbital elements database. Project funded principally by NASA grant NAG5-4741, and in part by the Lowell Observatory endowment. For more information, visit the URL `http://www.naic.edu/~nolan/astorb.html`.

[CG91]   A. Celletti and A. Giorgilli. On the stability of the Lagrangian points in the spatial Restricted Three Body Problem. *Celestial Mech.*, 50(1):31–58, 1991.

[CGL00]   A. Celletti, A. Giorgilli, and U. Locatelli. Improved estimates on the existence of invariant tori for Hamiltonian systems. *Nonlinearity*, 13:397–412, 2000.

[DDB67]   A. Deprit and A. Deprit-Bartolome. Stability of the triangular Lagrangian points. *Astron. J.*, 75(2):173–179, 1967.

[dlLGJV03]   R. de la Llave, A. González, À. Jorba, and J. Villanueva. KAM theory without action-angle variables. Preprint, 2003.

[GDF⁺89]   A. Giorgilli, A. Delshams, E. Fontich, L. Galgani, and C. Simó. Effective stability for a Hamiltonian system near an elliptic equilibrium point, with an application to the restricted three body problem. *J. Differential Equations*, 77:167–198, 1989.

[Gio95]   A. Giorgilli. Quantitative methods in classical perturbation theory. In A.E. Roy and B.D. Steves, editors, *From Newton to chaos: modern techniques for understanding and coping with chaos in N–body dynamical systems*. Plenum Press, New York, 1995.

[GJ01]   F. Gabern and À. Jorba. A restricted four-body model for the dynamics near the Lagrangian points of the Sun-Jupiter system. *Discrete Contin. Dyn. Syst. Ser. B*, 1(2):143–182, 2001.

[GL97a]   A. Giorgilli and U. Locatelli. Kolmogorov theorem and classical perturbation theory. *J. of App. Math. and Phys. (ZAMP)*, 48:220–261, 1997.

[GL97b]   A. Giorgilli and U. Locatelli. On classical series expansion for quasi–periodic motions. *MPEJ*, 3(5):1–25, 1997.

[GMS02]   G. Gómez, J.M. Mondelo, and Simó S. Refined Fourier analysis: procedures, error estimates and applications. Preprint, 2002.

[Grö60]   W. Gröbner. *Lie–Reihen und Ihre Anwendungen*. Springer Verlag, Berlin, 1960.

[GS97]   A. Giorgilli and C. Skokos. On the stability of the Trojan asteroids. *Astron. Astrophys.*, 317:254–261, 1997.

[Kol54]   A.N. Kolmogorov. On the persistence of conditionally periodic motions under a small change of the Hamilton function. *Dokl. Acad. Nauk. SSSR*, 98(4):527–530, 1954.

[KSW96]   H. Koch, A. Schenkel, and P. Wittwer. Computer-assisted proofs in analysis and programming in logic: a case study. *SIAM Review*, 38(4):565–604, 1996.

[Las95]   J. Laskar. Frequency map analysis of an Hamiltonian system. In *AIP Conf. Proc. of the* Workshop on nonlinear dynamics in particle accelarators, *Arcidosso (Italy), 1994*, volume 344, pages 130–159, 1995.

[Las99]   J. Laskar. Introduction to frequency map analysis. In C. Simó, editor, *Hamiltonian Systems with Three or More Degrees of Freedom*, NATO ASI, pages 134–150. Kluwer, Dordrecht, 1999.

[Leo62]   A.M. Leontovich. On the stability of the Lagrange periodic solutions of the restricted problem of three bodies. *Soviet Math. Dokl.*, 3:425–428, 1962.

[LG00]   U. Locatelli and A. Giorgilli. Invariant tori in the secular motions of the three–body planetary systems. *Celestial Mechanics and Dynamical Astronomy*, 78:47–74, 2000.

[Loc01]   U. Locatelli. Proof of a KAM theorem on the existence of invariant tori close to an equilibrium point. Quaderni del Dipartimento di Matematica 5, Univ. Milan, 2001.

[LR01]   J. Laskar and P. Robutel. High order symplectic integrators for perturbed Hamiltonian systems. *Celestial Mech.*, 80:39–62, 2001.

[Mar71]   A.P. Markeev. Stability of the triangular Lagrangian solutions of the restricted three-body problem in the three-dimensional circular case. *Soviet Astronom. AJ*, 15:682–686, 1971.

[Mar73]   A.P. Markeev. On the stability problem for the Lagrange solutions of the restricted three-body problem. *J. Appl. Math. Mech.*, 37:713–717, 1973.

[MG95]   A. Morbidelli and A. Giorgilli. Superexponential stability of KAM tori. *J. Statist. Phys.*, 78(5–6):1607–1617, 1995.

[Mos62]   J. Moser. On invariant curves of area-preserving mappings of an annulus. *Nachr. Akad. Wiss. Göttingen Math.-Phys. Kl. II*, 2:1–20, 1962.

[MS81]   R. McKenzie and V. Szebehely. Nonlinear stability around the triangular libration points. *Celestial Mech.*, 23(3):223–229, 1981.

[MS86]   K. R. Meyer and D. S. Schmidt. The stability of the Lagrange triangular point and a theorem of Arnold. *J. Differential Equations*, 62(2):222–236, 1986.

[Nek77]   N.N. Nekhoroshev. An exponential estimate of the time of stability of nearly-integrable Hamiltonian systems. *Russian Math. Surveys*, 32:1–65, 1977.

[PM03]   R. Pérez-Marco. Convergence or generic divergence of the Birkhoff normal form. *Ann. of Math. (2)*, 157(2):557–574, 2003.

[Pös82]   J. Pöschel. Integrability of Hamiltonian systems on Cantor sets. *Comm. Pure Appl. Math.*, 35:653–695, 1982.

[RL01]   P. Robutel and J. Laskar. Frequency map and global dynamics in the Solar System I. *Icarus*, 152:4–28, 2001.

[SD00]   C. Skokos and A. Dokoumetzidis. Effective stability of the Trojan asteroids. *Astron. Astrophys.*, 367:729–736, 2000.

[Sev03]   M.B. Sevryuk. The classical KAM theory at the dawn of the twenty-first century. *Moscow Math. J.*, 3(3):1113–1144, 2003.

[Sim89]   C. Simó. Estabilitat de sistemes Hamiltonians. *Mem. Real Acad. Cienc. Artes Barcelona*, 48(7):303–348, 1989.

[SWW00]   A. Schenkel, J. Wehr, and P. Wittwer. Computer-assisted proofs for fixed point problems in sobolev spaces. *MPEJ*, 6(3):1–67, 2000.

[Sze67]   V. Szebehely. *Theory of Orbits*. Academic Press, 1967.